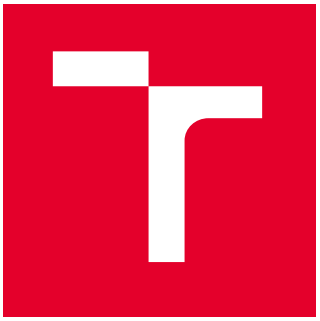

BRNO UNIVERSITY OF TECHNOLOGY

VYSOKÉ UČENÍ TECHNICKÉ V BRNĚ

FACULTY OF ELECTRICAL ENGINEERING AND COMMUNICATION

FAKULTA ELEKTROTECHNIKY
A KOMUNIKAČNÍCH TECHNOLOGIÍ

DEPARTMENT OF MICROELECTRONICS

ÚSTAV MIKROELEKTRONIKY

INTEGRATION OF LASER ABLATION INTO THE WORKFLOWS OF FIB-SEM SYSTEMS

INTEGRACE LASEROVÉ ABLACE DO PRACOVNÍCH POSTUPŮ SYSTÉMŮ FIB-SEM

MASTER'S THESIS
DIPLOMOVÁ PRÁCE

AUTHOR — **Ing. Jakub Valenta**
AUTOR PRÁCE

SUPERVISOR — **Ing. Martin Búran**
VEDOUCÍ PRÁCE

BRNO 2023

BRNO UNIVERSITY OF TECHNOLOGY
FACULTY OF ELECTRICAL ENGINEERING AND COMMUNICATION

Master's Thesis

Master's study program **Microelectronics**

Department of Microelectronics

Student: Ing. Jakub Valenta ***ID:*** 195459

Year of study: 2 ***Academic year:*** 2022/23

TITLE OF THESIS:

Integration of laser ablation into the workflows of FIB-SEM systems

INSTRUCTION:

Analyze the available information sources and develop a theoretical research on the given topic. Focus on the physical nature of the process and evaluate how various sources of electromagnetic radiation will affect different types of samples. Specify as many types of samples as possible to which the procedure may be applied (with regard to their use in the semiconductor industry) and evaluate how a specific type of electromagnetic radiation will manifest when processing these samples. Test the theoretical assumptions in practice, select the most interesting samples from the semiconductor segment, choose and experimentally verify the most suitable settings of process parameters in relation to the type of sample. Evaluate the results achieved and provide ideas for improvement.

RECOMMENDED LITERATURE:

Dle doporučení vedoucího práce.

Date of project specification: 6.2.2023 ***Deadline for submission:*** 23.5.2023

Supervisor: Ing. Martin Búran

doc. Ing. Lukáš Fujcik, Ph.D.
Chair of study program board

VYSOKÉ UČENÍ TECHNICKÉ V BRNĚ
FAKULTA ELEKTROTECHNIKY A KOMUNIKAČNÍCH TECHNOLOGIÍ

Diplomová práce

magisterský navazující studijní program **Mikroelektronika**

Ústav mikroelektroniky

Student: Ing. Jakub Valenta ***ID:*** 195459

Ročník: 2 ***Akademický rok:*** 2022/23

NÁZEV TÉMATU:

Integrace laserové ablace do pracovních postupů systémů FIB-SEM

POKYNY PRO VYPRACOVÁNÍ:

Proveďte analýzu dostupných informačních zdrojů a vypracujte teoretickou rešerši na uvedené téma. Zaměřte se na fyzikální podstatu procesu a zhodnoťte, jak se budou projevovat různé zdroje elektromagnetického záření na různé typy vzorků. Vyspecifikujte co největší množství typů vzorků, kterých se daný postup může týkat (vzhledem na použití v polovodičovém průmyslu) a zhodnoťte, jak se při obrábění těchto vzorků projeví specifický typ elektromagnetického záření. Teoretické předpoklady odzkoušejte prakticky, vytipujte nejzajímavější vzorky z polovodičového segmentu, vyberte a experimentálně ověřte nejvhodnější nastavení procesních parametrů vzhledem k typu vzorku. Zhodnoťte dosažené výsledky, uveďte nápady ke zlepšení.

DOPORUČENÁ LITERATURA:

Dle doporučení vedoucího práce.

Termín zadání: 6.2.2023 ***Termín odevzdání:*** 23.5.2023

Vedoucí práce: Ing. Martin Búran

doc. Ing. Lukáš Fujcik, Ph.D.
předseda rady studijního programu

ABSTRACT

The aim of this diploma thesis is to verify the influence of different settings of a laser ablation system parametres on different types of microelectronic materials. The goal of the thesis is to describe the purpose of physical failure analysis in these structures and the method of how to solve them. The principles of the machining and imaging devices' functionality at the level of micro- or nanometer-sized structures are solved in this work. The subject of investigation is mainly the operational difference between ion beam and laser beam machining processes and its integration into the area of quality assurance. It is about the connection of laser devices with systems of ion and electron beams. The work also describes the results of experiments during which the analysis of defects of selected structures was carried out.

KEYWORDS

laser, ablation, scanning electron microscope, focused ion beam, electron, microscopy, quality assurance, quality control, defect, analysis

ABSTRAKT

Cílem této diplomové práce je ověření vlivu různých nastavení parametrů systému laserové ablace na různé typy mikroelektronických materiálů. Práce má za úkol popsat účel analýzy skrytých defektů v těchto strukturách a způsob jejich řešení. V rámci práce jsou řešeny principy funkce obráběcích a zobrazovacích zařízení na úrovni mikro- či nanometrových velikostí struktur. Předmětem zkoumání je především operační rozdíl mezi procesy obrábění pomocí iontového svazku a pomocí laserového paprsku a jeho integrace do oblasti zajištění kvality. Jde o propojení laserových zařízení se systémy iontových a elektronových svazků. V práci jsou také popsány výsledky experimentů, během kterých byla provedena analýza defektů vybraných struktur.

KLÍČOVÁ SLOVA

laser, ablace, skenovací elektronový mikroskop, fokusovaný iontový svazek, elektron, mikroskopie, zajištění kvality, řízení kvality, defekt, analýza

ROZŠÍŘENÝ ABSTRAKT

Každý vyráběný produkt je produkován s tím smyslem, aby plnil svůj účel a svou funkci v rámci na něj stanovených požadavků. Tyto požadavky buď stanovuje platná legislativa nebo trh, tedy zákazník/odběratel. Pokud si zákazník stanoví na produkt nějaké požadavky, očekává, že budou výrobcem splněny. Aby toho výrobce dosáhl, musí vytvořit a dodržovat takzvaný systém řízení (managementu) kvality. Takový systém, pokud je správně nastaven a dodržován, umožní kontrolovat výrobní procesy, vyhledávat neshody a nesrovnalosti, zlepšovat a zdokonalovat, a hlavně reagovat na požadavky přicházející zvenku. Systém řízení kvality pomáhá snižovat výrobní a servisní náklady, neboť se jedná především o preventivní procesy, čímž přispívá ke zvedání spokojenosti (důvěryhodnosti) a zisků při současném omezení počtu vadných výrobků. To vše se samozřejmě týká i oblasti výroby mikroelektronických a polovodičových struktur.

Součástí řízení kvality je analýza chyb a defektů. Tyto se samozřejmě vyskytují (resp. mohou vyskytovat) i v mikroelektronických strukturách. Integrace a miniaturizace elektronických struktur sice umožňuje tvorbu složitých a výkonných zařízení s ohromnou výpočetní silou, zároveň však vede k situaci, že je čím dál obtížnější takové chyby a vady odhalit. Struktury mohou totiž být (a bývají) skryté v různých součástkových pouzdrech, navíc, jak už název napovídá, nabývají mikroskopických až nanoskopických rozměrů a jsou tedy pouhým okem či běžnou technikou nepozorovatelné. Navíc pro tyto účely a většinu vzorků nebyla zatím nalezena jiná možnost analýzy než destruktivní formou. K analýze defektu je nutné odebrat část materiálu (pouzdra, struktury...). K tomu je však potřeba velmi přesných nástrojů.

Pokud se ale podaří defekt odhalit, lokalizovat a zpřístupnit, přichází další problém v podobě jeho zobrazení a analýze. Běžné zobrazovací přístroje jsou často v této oblasti téměř nepoužitelné, především z důvodu principu, na kterém jsou založené. Pokud je nutné zobrazovat struktury o velikostech mikro- až nanometrů, musí být použita výkonnější zařízení – např. elektronový mikroskop a jeho alternativy. Díky principu, na kterém pracují, jsou schopny zobrazovat a zvětšovat právě takto malé struktury, díky čemuž je možná analýza právě takovýchto typů objektů a vzorků.

Tato práce se zabývá právě experimentální analýzou defektů v rámci zajištění kvality mikroelektronických struktur a integrací nových postupů do již ověřených a zavedených. Pokud je třeba pro odhalení defektu odebrat „velké množství materiálu“, mohou být některé procesy pro takové účely velmi časově náročné. Za použití laserového pulsního zařízení je možné tyto procesy urychlit. Na základě rešerše tak tato práce popisuje, jakým způsobem daná zařízení pracují, jejich výhody a nevýhody, a také jak je možné takováto zařízení použít právě v rámci systému zajištění kval-

ity. Stejně tak se práce zabývá dalšími zmíněnými úrovněmi analýzy defektů, tedy přípravou vzorku, jeho leštění iontovým svazkem a následným zobrazením pomocí elektronového mikroskopu. Formou několika experimentů byla ověřena účinnost a efektivita laserové ablace v tomto oboru ve srovnání s kopáním pomocí iontového svazku (který jde využít v rámci těchto procesů mnohem elegantněji).

Experimenty v této práci byly provedeny na základě jednotného pracovního postupu. Různé vytipované mikroelektronické struktury a vzorky byly vloženy do komory laserového zařízení, kde proběhla ablace a odhalení interních struktur. Parametry laseru byly většinou nastavovány iterativně s ohledem na konkrétní materiály. Takto vytvořené průřezy byly přesunuty do komory elektronového mikroskopu s iontovým tubusem, kde některé vzorky podstoupily „leštění“ iontovým svazkem. Upravené vzorky byly následně analyzovány pomocí elektronového svazku, přičemž byly hledány anomálie, defekty a další netypické artefakty.

Pomocí těchto experimentů byl ověřován vliv elektromagnetického záření na různé typy vzorků a materiálů. Rovněž bylo hledáno nejlepší nastavení procesních parametrů pro konkrétní typy vzorků, to se ovšem ale pro každý vzorek lišilo. Bylo zjištěno, že při laserové ablaci záleží na nastavení každého konkrétního parametru a jejich vzájemnou kombinaci. Ve druhé části experimentů proto bylo toto nastavení hledáno pro každý vzorek zvlášť iterativně, než bylo dosaženo ideálního výsledku. V průběhu analýz pak bylo nalezeno dostatek mikroelektronických defektů a anomálií, které bylo možné analyzovat.

VALENTA, Jakub. *Integration of laser ablation into the workflows of FIB-SEM systems*. Brno: Brno University of Technology, Faculty of Electrical Engineering and Communication, Department of Microelectronics, 2023, 75 p. Master's Thesis. Advised by Ing. Martin Búran

Author's Declaration

Author:	Ing. Jakub Valenta
Author's ID:	195459
Paper type:	Master's Thesis
Academic year:	2022/23
Topic:	Integration of laser ablation into the workflows of FIB-SEM systems

I declare that I have written this paper independently, under the guidance of the advisor and using exclusively the technical references and other sources of information cited in the paper and listed in the comprehensive bibliography at the end of the paper.

As the author, I furthermore declare that, with respect to the creation of this paper, I have not infringed any copyright or violated anyone's personal and/or ownership rights. In this context, I am fully aware of the consequences of breaking Regulation § 11 of the Copyright Act No. 121/2000 Coll. of the Czech Republic, as amended, and of any breach of rights related to intellectual property or introduced within amendments to relevant Acts such as the Intellectual Property Act or the Criminal Code, Act No. 40/2009 Coll. of the Czech Republic, Section 2, Head VI, Part 4.

Brno ....

author's signature*

*The author signs only in the printed version.

ACKNOWLEDGEMENT

I would like to take this opportunity to thank the supervisor of my diploma thesis, Mr. Ing. Martin Búran, for his valuable time, very kind and friendly approach, patience and professional consultation with stimulating suggestions and advises, which helped me a lot during the time of writing this thesis. I am glad that I could deal with my topic with him as my advisor.

Contents

List of Figures

List of Tables

Introduction

The production process of any product is divided into several stages, each of which is undoubtedly important for the final product to fulfill its function within the requirements set for it. Ensuring sufficient quality is also one of these parts of the production process. Thanks to quality management, production and service costs can be reduced due to improvements to the production process itself and thus also the reduction of the number of defective pieces of the product, and the credibility of the manufacturer in the eyes of the customer also increases, which contributes to greater profits. Due to the topic, this work will focus on the production of microelectronic and semiconductor structures.

One part of quality management is defect analysis. The ever greater integration and shrinking of the dimensions of microelectronic structures leads to a situation where these defects are increasingly difficult to detect. On the one hand, they can be encapsulated in various component packages, on the other hand, they can be of microscopic to nanoscopic dimensions. Unfortunately, no other than destructive form of analysis has yet been introduced for these purposes – it is often possible to get to the defect only by removing part of the material. For these purposes, however, very precise tools are needed, moreover, due to the dimensions of the analyzed structures, the "part of the material" is relatively of volume.

However, if the defect can be detected and made available, another problem arises, namely its observation and analysis. Conventional imaging devices are often almost unusable in this area, mainly because of the principle on which they are based. If structures with a size of a few micrometers or even nanometers need to be visualized, it is necessary to use more powerful devices – e.g. electron microscope and its alternatives. These systems are able to display just such small structures, thereby effectively assisting the analysis of objects that would otherwise be impossible to observe.

This work will thus be focused on the quality management system and the importance of its function with regard to the analysis of physical microscopic defects in microelectronic structures. Depending on this, the possibilities of microscopic milling and material removal will be discussed here, emphasizing the two currently used methods – laser ablation and ion machining. Furthermore, the thesis will introduce the principle of electron microscopy and scanning electron microscope. At the end, set of experiments will be carried out, during which the influence of different laser parameters on some electronic structures will be monitored and described.

1 Quality Assurance and Defect Analysis

During the manufacturing process of any product, it is necessary for the producer to ensure that the resulting product meets all the declared properties or requirements. Of course there is no exception when it comes to the production of semiconductor and other electronic components and devices. To ensure the specified quality of all manufactured devices, electrical and mechanical testing of samples is carried out at every level of their production, and that is from the level of initial designing (where testing requirements shall be set) to the level of distribution of the devices to end customers. This process is called *Quality Assurance and Quality Control*. In this chapter, Quality assurance and Quality control systems will be defined and described, as they include a number of actions that will be the subject of the practical part of this paper.

1.1 Quality Assurance and Quality Control

The area of Quality assurance (usually abbreviated as *QA*) can be described as a science and/or ability of incorporating quality into the product manufacturing process so that only those products that meet the reliability requirements are delivered to customers. Thus, in other words, QA is any systematic process of determining whether a particular product sample meets specified quality requirements. As a result, customers can only be supplied with high-quality material which they can use for their purpose. Obeying QA principles build trust and loyalty with customers. The standards and procedures defined by a quality assurance program help prevent product defects way before they arise. [1] [2]

Quality Assurance is defined in ISO standards, specifically in the ISO 9000 set. It contains five standards about Quality Management systems (abbreviated as "QMS"). In these standards, one can find the fundamentals of QMS, quality management principles, requirements that organizations should fulfill, model for quality assurance in production and inspection etc.

Another term mentioned in this area is Quality control (usually abbreviated as "QC"). QC is a subset of QA and can be described as the process itself of maintaining the quality characteristics of the process and/or product within the specified and required limits. As part of quality management, the methods and procedures for control are established, to which the conditions of acceptance or rejection of the product are linked. Accepted material is processed countless times, stored and tested on several occasions as it passes throughout the production. This process is thus present in all parts of production. [1]

Fig. 1.1: The difference between Quality Assurance and Quality Control [3].

Both these terms are often confused. It is true that both processes share some similarities, their meanings can be completely distinguished though. As can be seen in Figure 1.1, quality control is a subset of the quality assurance set, and both components are further subsets of the overall quality management system.

QA includes a set of activities and procedures that are addressed from the early stage of product development to the final level of its life cycle end. It establishes principles and procedures for maintaining quality and requires compliance with technical standards defined by the company and other organizations. The quality assurance process is then process-oriented and is focused on improving the product development process and methods (easily said, it is a preventive process). QC, on the other hand, is a set of activities that are performed to verify that the final product meets the requirements set forth by QA. Quality control is focused on improving the product itself by finding flaws in the design and manufacturing process. It is therefore, in contrast to QA, a product-oriented process. [3] [4] [5]

1.2 Hidden Defects Analysis

The analysis of hidden defects and malfunctions is also part of the quality assurance and quality control processes. At the current level of miniaturization and integration of microelectronic and semiconductor devices, it is often difficult to detect some functional defects. On top of that, these are often hidden in deeper areas of the structures by conventional methods. In order to ensure good quality and reliability levels, advanced imaging tools are needed. This will be dealt with in chapter 2.

In this section, the process of hidden defect analysis and its importance will be explained in more detail.

The analysis of physical defects (which is commonly referred to as the Failure Analysis) is a fundamental way to rule out manufacturing process deviations that are counterproductive in terms of reliability and customer satisfaction. The goal of this analysis is to determine the root cause of hidden defects or deviations of the required parameters, which will allow the necessary corrective measures to be taken in order to prevent an occurrence of these deviations in the future. It is necessary for these defects to be located and analyzed. For these purposes, it is possible to use advanced technology such as imaging using electron microscopy (see section 2.2), focused ion beam (see section 2.3) or, for example, transmission (TEM) or X-ray microscopy (XRM). [6]

Failure analysis is a highly demanded practice in companies that manufacture microelectronic products. Such products or structures include: [7]

- Micro Electro-Mechanical Systems (MEMS)
- through-silicon vias
- solder ball arrays
- bonding micro-wires
- etc.

During the analysis of these structures the following defects are localized and analyzed:

- design flaws
- structural defects
- cracks
- voids
- faulty internal contacts
- under-fillings
- and more

Locating these defects normally requires making a cross-section in the structure as no non-destructive method has yet been established that would be reliable enough to safely locate and visualize the defect. Due to the large integration and encapsulation of individual structures these days, these cuts must be made often to a depth/width of several hundred microns. [6]

2 Electron Microscopy

In technological practice, it is often necessary to observe and examine objects that are of very small dimensions. Since the resolving power of the human eye is not large enough for these purposes, various magnifying devices are often used. These devices might be called optical magnifiers. Some sufficiently large objects can be observed with an ordinary optical microscope, which uses a source of visible light radiation and a system of optical lenses that ensure sufficient optical magnification. The object magnified in this way can then be observed through the eyepieces which are also part of the microscope. However, some objects reach much smaller dimensions, which even an optical microscope is insufficient to enlarge.

Electron microscopy technology can be then used to observe such objects. Since this paper is focused on workflows that use aforementioned technology, its general principle and its division into individual types will be described in more detail in the following sections.

2.1 General Principle of Electron Microscopy

As it was already mentioned, electron microscopy (EM) is a technique for obtaining very high resolution images of objects or samples. Resolution, the shortest distance between two different points that can be distinguished by the observer, is determined (physical principle) by the wavelength of the particles used, or more precisely by half of this wavelength. In optical microscopy, visible light with an average wavelength of 550 nm is used as an illumination radiation, so it is theoretically possible to distinguish two points approximately 250 nm apart. [8]

In contrast, electron microscopy uses an electron instead of a photon, the wavelength of which is determined based on the accelerating voltage applied to it according to the formula for the "De Broglie wavelength" (see Equation 2.1),

$$\lambda = \frac{h}{p} = \frac{h}{\sqrt{2m_e eU}}, \tag{2.1}$$

where λ denotes the wavelength, h the Planck constant, p the momentum of the electron, m_e the mass of the electron, e the elementary charge, and U the accelerating voltage [9].According to this formula, using an accelerating voltage of 10 kV it is possible to achieve a resolution of half the value of 0.0123 nm. Thanks to this, it is then possible to visualize and observe the structure of much smaller samples.

However, it is also good to mention the disadvantage of electron microscopy, or more precisely using an electron beam for imaging. Since it is desired to achieve

a very high resolution, precision is required in electrons hitting the correct spot on the examined sample. If air were present in the parts of the microscope through which the electrons travel, the electron beam would be greatly distorted and the observation results would not be satisfactory. Therefore, it is necessary to maintain the pressure level in such parts at vacuum-close values.

Electron microscopy could be divided into two branches: [10]

- Scanning Electron Microscopy (SEM)
- Transmission Electron Microscopy (TEM)

Both mentioned technologies work on a partially different principle and are used to display different properties of the observed samples.

A transmission electron microscope is used to observe very thin samples through which the emitted electrons pass (have sufficient energy) in order to produce an image on a fluorescent screen placed behind the sample.

In contrast, the scanning electron microscope uses the emission of secondary and back-scattered electrons from the surface of the examined sample after the impact of the primary electron. SEM is characterized by a large depth of focus, thanks to which it is able to provide detailed images of the surface of the observed sample. To do so this, it uses a set of different detectors. Considering the topic of this paper, it will continue to deal with SEM technology only, which will be described in more detail in the next chapter.

2.2 Scanning Electron Microscopy

Any scanning electron microscope is generally composed of five basic components: [11]

- electron source (electron gun)
- electron column
- electromagnetic lenses
- viewing system
- specimen holder

The electron microscope is also defined by certain characteristics. Perhaps the single most important characteristic of the source is *brightness*, which characterizes the electron current density of the beam and the angle into which the current is emitted. This eventually determines the resolution, contrast and signal-to-noise capabilities of the imaging system.

In the following subsections, the aforementioned items will be described in more detail. However SEM also uses a lot of control software, which is unfortunately typical for each manufacturer and cannot be described in detail. These software systems, although they probably work on the same principle, are proprietary and will not be the subject of this paper.

2.2.1 Electron Sources in SEM Systems

There are three key types of electron sources used in scanning electron microscopy, each of which has different advantages and disadvantages. [12] These types are displayed in Figure 2.1 and include:

- Tungsten guns
- LaB_6 or CeB_6 guns
- FEG (Field Emission Gun)

The tungsten gun is composed of a tungsten filament, an anode and a Wehnelt cylinder, which together form a very stable source of electrons. The tungsten filament is hairpin-shaped and is heated to a temperature of approximately 2700 K, it then fulfills the function of a cathode. If a high potential difference is applied between the cathode and the anode, electrons are extracted from the tungsten filament and are accelerated towards the anode by this potential. The Wehnelt cylinder is placed near the cathode and a negative voltage is applied to it. This creates an electrostatic field, due to which electron emission from most of the cathode area is suppressed and concentrated only to a small area on the tip. The anode is then placed under the Wehnelt cylinder. In the middle of the anode there is a hole through which electrons fly at high speed and are directed further into the column. Tungsten filaments are the cheapest sources, but at the cost of limited lifetime and resolution.

LaB_6 (or CeB_6) guns also work on the basis of thermoemission of electrons from a cathode, and are composed of the crystal of this material. These electron sources offer approximately ten times higher brightness and a longer lifetime, but they are more demanding on the required vacuum level. This makes the price of the microscope higher.

The last of the typical sources of electrons is the so-called FEG, which is an abbreviation for *Field emission gun*. This gun is composed of a sharp tungsten tip from which electrons are emitted by a very strong electric field. This is the most expensive type of electron source, but they achieve the best results in terms of resolution and brightness and analytical capabilities. Unlike previous types of guns, it does not use thermoemission, but rather electromagnetic emission of electrons, thanks to

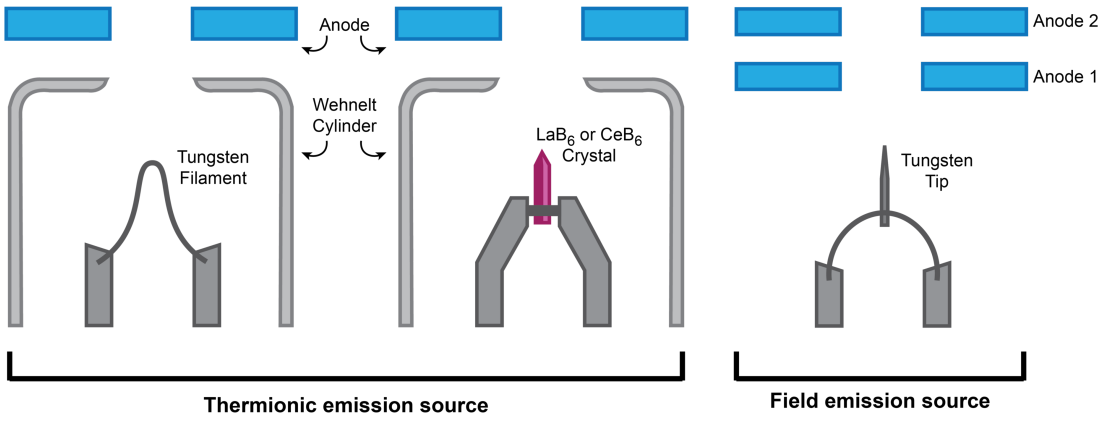

Fig. 2.1: The most used types of electron sources in SEM. [13]

which it achieves a higher current of the electron beam despite the small area of the emitter. [12] [13]

2.2.2 Electron Column as a Part of SEM

Another part of the electron microscope is the electron column, inside of which there are electronics focusing and directing the electron flying from the cathode tip towards the sample being examined. In essence, these are the elements analogous to those that can be found in an optical microscope (lens system). Instead of a light source, the aforementioned electron source is used here (see subsection 2.2.1), transparent glass optical lenses are replaced by electromagnetic or electrostatic lenses and stigmators. Using deflecting electromagnetic and electrostatic lenses, the electron beam is focused into an almost parallel beam and focused on the observed area of the sample. It is also possible to find apertures in the column, the function of which is to let through only that part of the electron beam of which the direction is closest to the straight direction relative to the axis. A cross-section of the entire electron column is shown in Figure 2.2. [12]

Only electromagnetic lenses are used in SEM systems, due to their much lower aberrations (deviations) compared to electrostatic ones. Even so, these lenses show worse performance than classic optical lenses. [14]

2.2.3 Types of Electromagnetic Lenses in SEM

Unlike the TEM system, the focusing systems in SEM consist of only two types of electromagnetic lenses: [15]

- condenser lens
- objective lens

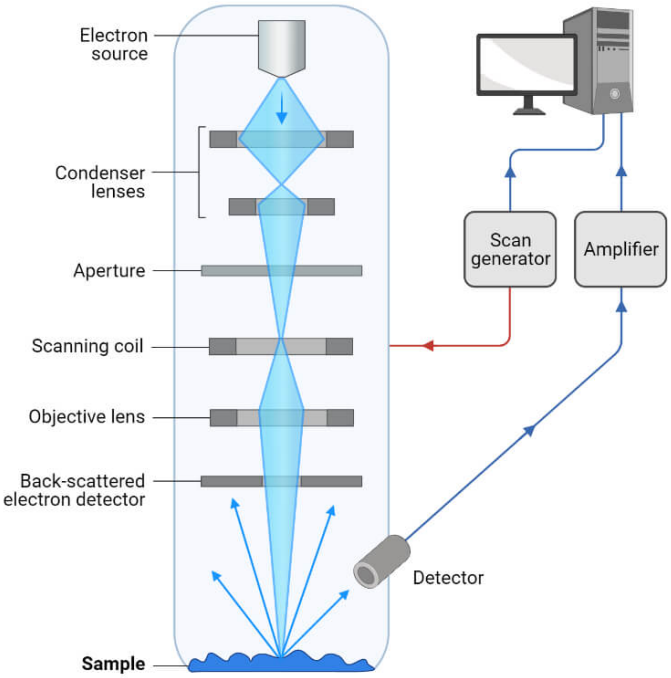

Fig. 2.2: The internal structure of the electron column in SEM technology [11].

Each of these types is designed for a different purpose and is located in a different part of the electron column. Objective lenses are then divided into three basic subtypes and each of these types having their own advantages/disadvantages. These subtypes differ essentially only in the position of the observed sample relative to the objective lens, depending on whether the sample is located inside or outside the objective lens. The function and principle of each of these types and subtypes will be described in the following chapters.

Condenser Lenses

One to three lenses of this type are usually used in SEM systems. After the electron (or electron beam) is emitted from the cathode, it is accelerated towards the anode with an opening through which it flies. During its journey through the column, it is conically dispersed due to the voltage at the anode and it needs to be focused. [16]

Condenser lenses are thus placed in the upper part of the tube and serve to concentrate the beam; they determine its size and thus also the final resolution. After a certain distance, the electron beam disperses again and needs to be re-directed by another condenser lens or directly by the objective lens. This process can also be aided by apertures located behind the lenses, which are designed to let only that part of the focused beam through that moves most parallel to the axis and thus has the lowest degree of deviation. [15]

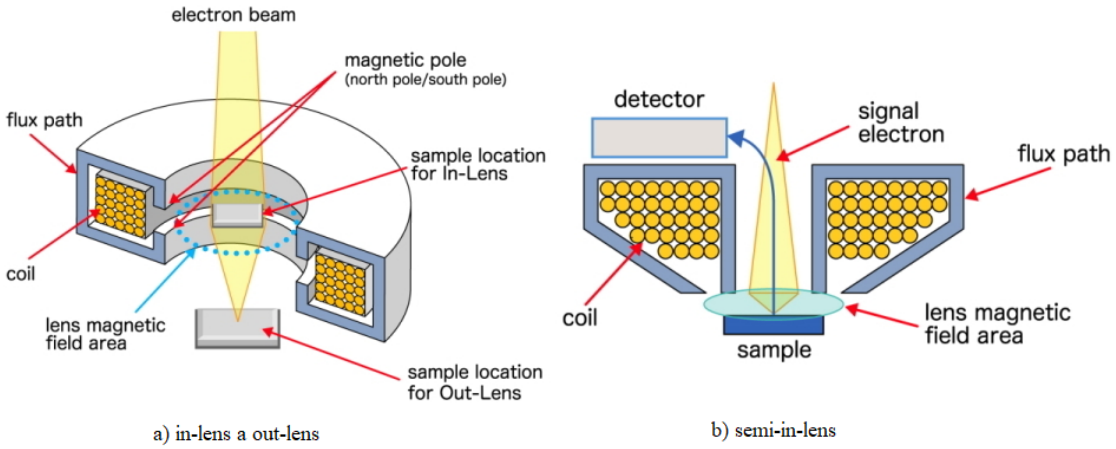

Fig. 2.3: Structure of objective lenses and depiction of sample position by type a) out-lens and in-lens a b) semi-in-lens. [14]

Types of Objective Lenses

The objective lens is the last lens directing the movement of the electron beam in the tube. It focuses the electron beam directly on the surface of the observed sample. Because objective lenses are stronger and more powerful than condenser lenses, and because higher current flows through them, they need to be cooled frequently. Their size must also be adjusted so that the lenses provide space for scanning coils (see Figure 2.3), stigmators and an aperture limiting the thickness of electron beam to a thin line. [12]

The objective lenses thus fulfill the function of final focusing on the sample. There are 3 basic subtypes:

- pinhole objective lens
- immersion objective lens
- snorkel objective lens

These kinds of objective lenses differ in the position of the observed sample, based on which the lenses then work. With the first mentioned is the position *"out-lens")*, the second is the *"in-lens"* position and the last one is a combined position, the so-called *"semi-in-lens"* (see Figure 2.3). [15]All aforementioned types will be described in the following paragraphs.

Pinhole Objective Lens The most basic objective lens is the so-called asymmetrical pinhole lens, or also the conical lens (see Figure 2.4a). This lens is used for situations when the sample is situated in the *out-lens* position. The last polepiece of the electromagnet forms a very small opening, which prevents the magnetic field

from reaching the outside of the lens. This preserves a magnetic field-free region above the sample, allowing good detection of secondary electrons (abbreviated as "SE", see section 2.2.4). [17] The advantage of this lens is that the sample size is limited only by the size of the chamber itself and that a high depth of field of the resulting image can be achieved. A significant disadvantage is the need to hold the sample very close to the polepiece, as the amount of deviations from the raster point increases with larger working distances, which worsens the quality of the final image.

Immersion Objective Lens Another type of objective lens is the immersion lens used for situations of samples in the *in-lens* position (see Figure 2.4b). The small sample is placed directly into the area inside the lens itself. It thus provides the lowest focal length. Since the aberration of the objective is directly proportional to the focal length, this design provides the lowest deviations of the electron beam, and therefore the highest resolution and brightness of the resulting image. The detection of secondary electrons in this lens takes advantage of the fact that these electrons can spiral up in a strong magnetic field to the detector, which is located above the lens. In addition, secondary electrons can be very well separated from back-scattered electrons ("BSE", see section 2.2.4) using this system. [14] However, the disadvantage is the necessity of very small dimensions of the observed sample.

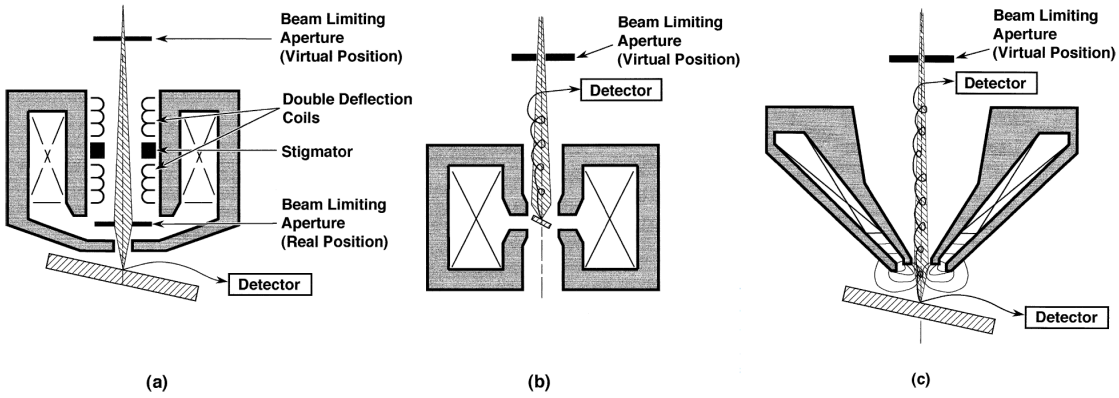

Fig. 2.4: Cross-section of three types of objective lenses: a) pinhole lens, b) immersion, c) snorkel. [14]

Snorkel Objective Lens The last lens is the so-called "snorkel" or single-pole lens (see Figure 2.4c). Its function is based on the fact that a strong magnetic field also extends from the polepiece directly into the sample area. [14] This lens has been designed to combine the best features of the previously mentioned lenses. It provides low electron beam aberrations similar to an immersion lens, while the sample size is not limited by the size of the lens itself like with a pinhole lens. In addition, it

allows the use of both types of secondary electron detectors (both inside and outside of the column), thus offering flexibility in the processing of the final image of the sample. [14]

2.2.4 Types of Signals Used in SEM

After the electron beam is emitted from the cathode and accelerated and directed during its journey through the column, it impacts on the sample under observation, which is typically situated in a vacuum chamber. As the incident electrons have high energy, physical processes occur after their impact, the result of which are signals. These signals are then processed in various ways, thanks to which it is possible to construct an (magnified) image of the observed sample. The most important, commonly used signals are: [18]

- Secondary electrons (SE)
- Back-scattered electrons (BSE)
- Energy-dispersive X-ray (EDX)

Each of these signals originates at a different depth below the surface of the sample and thus carries different information about it (shown in Figure 2.5). Of course, there are more signals arising after the impact of an electron on the sample (Auger electrons, light radiation...), but their detection is not widespread to such an extent in this field. Regarding the topic of this thesis, only the first two mentioned types of signals will be described in more detail in the following subsections. It is because the process does not use the other signals.

Secondary Electrons

One of the main signals used in scanning electron microscopy is the signal formed by so-called secondary electrons (SE). These electrons are the products of ionization [20]and they are electrons from the outer shell of the atom of the observed sample. If an electron from the electron beam hits an atom of the sample inelastically, excitation of the electron from the atomic shell can occur. Such an electron acquires sufficient kinetic energy to leave the shell of the atom and eventually escape from the surface of the sample, where it can subsequently be detected as a signal. [18]

Secondary electrons have a lower energy, which normally ranges between 2 eV and 10 eV (however, all electrons with energy $E < 50$ eV are considered SE). Due to the fact that these electrons originate from a region close to the sample surface, they carry significant information about the surface topography. [21]

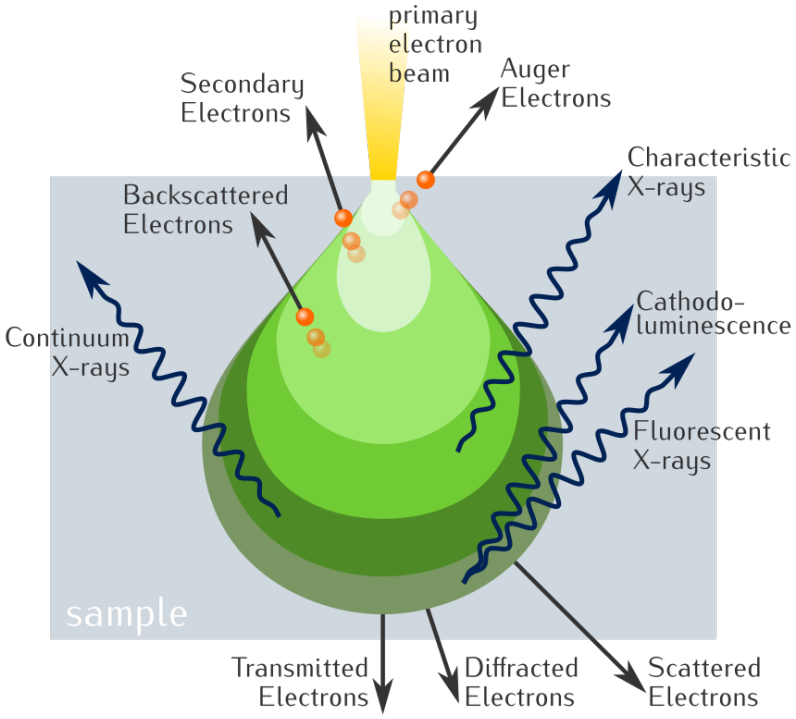

Fig. 2.5: Types of signals formed in SEM after the impact of an electron on the observed sample [19]

Back-scattered Electrons

Back-scattered electrons (*BSE*) originate from a broad region within the interaction volume. These are beam electrons that entered the sample and due to elastic collisions and scattering (and thus low energy losses), their trajectory was changed so that they left the sample surface again. Since these electrons are of much higher energy than SE, they originate from much deeper parts of the sample (which also causes lower resolution and brightness).

The number of back-reflected electrons captured by the detector directly depends on the atomic number of the examined sample. [22] It is because larger atoms (with a greater atomic number) have a higher probability of producing an elastic collision (greater cross-sectional area). Due to this phenomenon, these electrons carry a valuable signal about its chemical composition. BSEs also transfer a large amount of energy during their trajectory, which causes the production of other secondary radiations (e.g. the already mentioned characteristic X-rays), which carry other important information about the observed sample and the impurities in its volume.

2.2.5 Detectors Used for Imaging in SEM

Electron detectors are used to collect signals generated from the sample as a result of interaction of the electron beam with the sample surface. In SEM systems, two different principles are commonly used for signal detection. The first principle is the conversion of signal electrons into the form of photons using a scintillating material and a photomultiplier and subsequently converting them back into an electrical signal. The second principle is based on the generation of electron – hole pairs in a semiconductor, which can be separated and detected before recombination. However, there is also a third principle which uses a channel electron multiplier. It converts the signal electrons after they impact on the input into secondary electrons and multiplies them afterwards. [21]

The most used are the first two mentioned principles, which will also be described below.

Detection Using a Scintillator

The most common and widely used electron detector found in SEM systems is the Everhart – Thornley detector (commonly abbreviated as *ETD*). [14] ETD can be used for both SE and BSE detection and its schematic is shown in Figure 2.6. The function of this detector is based on the following sequence:

1. The electron beam impacts on the surface of the sample. SE or BSE generation occurs.
2. Depending on the voltage, the SE and/or BSE are attracted to the scintillator grid[1].
3. Electrons are accelerated by a voltage of up to 12 kV on the scintillator. It generates a photon upon impact.
4. The photon is conducted through a glass tube towards the photocathode, where the photon is converted into a photoelectron upon hit.
5. Photoelectrons are conducted and multiplied (up to a million times) by a photomultiplier until they hit the anode on the other side.
6. An electronic signal is generated that can be processed by other systems.

It is possible to connect the scintillator grid to a voltage from −50 V to about +300 V, thus determining whether SE or BSE will be detected. If the grid is connected to a positive voltage, this ensures a very effective detection of SE, in the case of a negative potential being connected, on the contrary, their detection is completely suppressed.

[1] If the grid voltage is negative, the BSEs are not really attracted. However, they have enough energy to overcome this potential barrier. [14]

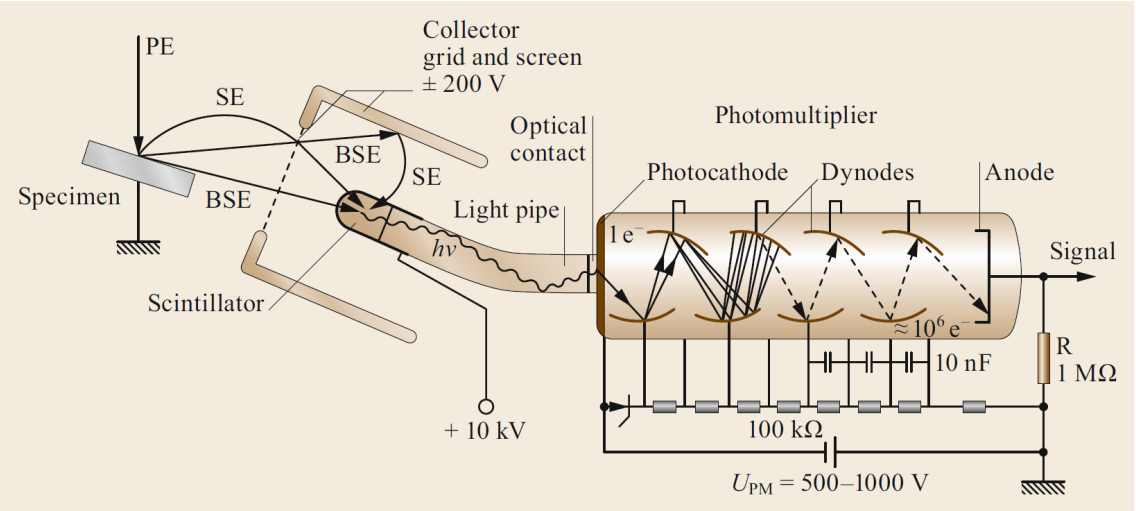

Fig. 2.6: Schematic picture of the Everhart-Thornley detector. [21]

Detection by Electron Pair Generation

Another of the detectors, which, however, is only used for BSE detection, is the semiconductor detector. The principle of its operation is based on the fact that an incident back-scattered electron with a high energy generates a large amount of electron-hole pairs in the structure of the detector. Given that the excitation energy in silicon is equal to $E = 3.6\,\text{eV}$ and BSEs impact on the detector with energy in the order of keV, there is a considerable amount of pairs generated in this way. In addition, if the PN junction is connected to a voltage source, these pairs are drew off by the electrodes before their recombination. Thanks to this, it is possible to convert the accumulated charge on the electrodes into a signal using a current amplifier and create the resulting image based on it. [23]

2.3 Focused Ion Beam (FIB)

Another technology, working on a very similar principle, can also be included in the topic of electron microscopy. These are systems working with a focused ion beam (usually abbreviated as “FIB”). Although these systems are largely similar to the already described SEM systems, there are also a number of differences between them, both in their principle and use. Since this work is to a certain extent concerned with the use of ion beams in the workflows of quality assurance, in this section the function and use for the analysis of defects and malfunctions will be described.

2.3.1 Principle of Operation of FIB Systems

As already indicated, FIB systems are composed and operate in a very similar way to SEM systems. The main difference is that they use a focused ion beam instead of an electron beam. In FIB systems, the ion beam is generated by a liquid metal ion source (usually abbreviated as "LMIS"). This source typically consists of a tungsten tip and a reservoir of source material. Gallium (Ga^+, as the ions used are positive) is most often used as a source material for several reasons: [24]

1. Low melting temperature $T_m = 29.8\,°C$, which minimizes the probability of reaction with the tungsten tip.
2. Low volatility at the melting temperature and thus a long service life of the source.
3. Low surface energy, which ensures viscous behavior.
4. The low evaporation pressure allows its use in pure form (no need to use it in the form of an alloy) and therefore provides a long service life - the liquid does not evaporate.
5. Excellent mechanical, electrical and vacuum properties.

After the ions are emitted from the LMIS, they are accelerated in the ion column (see Figure 2.7) and subsequently focused on the observed sample using electrostatic lenses. Here it is appropriate to point out that, unlike the electrons used in SEM, which are directed by electromagnetic lenses, the ions are much heavier. Therefore, the use of only electrostatic lenses come into consideration here, since the speed of the ions and thus the Lorentz force are lower. The electromagnetic lenses are therefore less effective.

The ion column contains, similarly to the electron tube, typically two types of lenses – condenser and objective. A condenser lens, again, directs the beam on its way through the comlumn, and an objective lens is used to focus the ion beam onto the observed sample area. Also there are stigmatizers used whose function is provided by octupole lenses (which also ensure scanning).

After the impact of the beam of primary ions on the surface of the sample, a small amount of material is sputtered. The implantation of high-energy heavy ions generates (*sputters*) secondary ions or neutral atoms. Among other things, secondary electrons (SE) are also produced. Using these secondary products of sputtering, it is possible, similar to SEM, to generate an image of the observed sample. [26]

At low beam currents, very little material is sputtered, and in these regimes the FIB can olso be used for imaging with resolutions down to 5 nm. However, if the beam current is set to higher values, a large amount of material is sputtered with high precision, which can afterwards be used in QA processing.

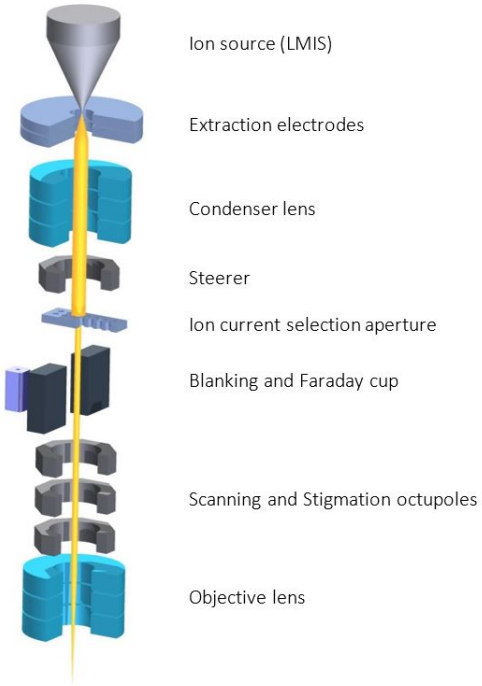

Fig. 2.7: Cross-section of the FIB system ion column [25]

2.3.2 Use of FIB Systems

As mentioned in the previous section, the accelerated ions are of a high energy and, due to their mass, have a much greater influence on the sample in the chamber in terms of material changes than electrons in SEM systems. After the impact of the ion beam on the surface of the sample, these ions enter the material of the sample and interact with it in various ways within the depth of penetration. The form of this interaction is strongly dependent on the energy with which the ions impact on the sample. These contain:

- sputtering of material
- implantation into the material
- amorphization of material
- volume change of material – swelling
- backscattering
- and other...

However, many of these interactions take place simultaneously and it is not possible to determine exactly which one dominates the process. [24]

These interactions can be used for many purposes in FIB technology. Using low-energy ions, FIB can be used, like SEM, to display information about the topography of a sample. From the perspective of damage to the original surface, it is obvious that

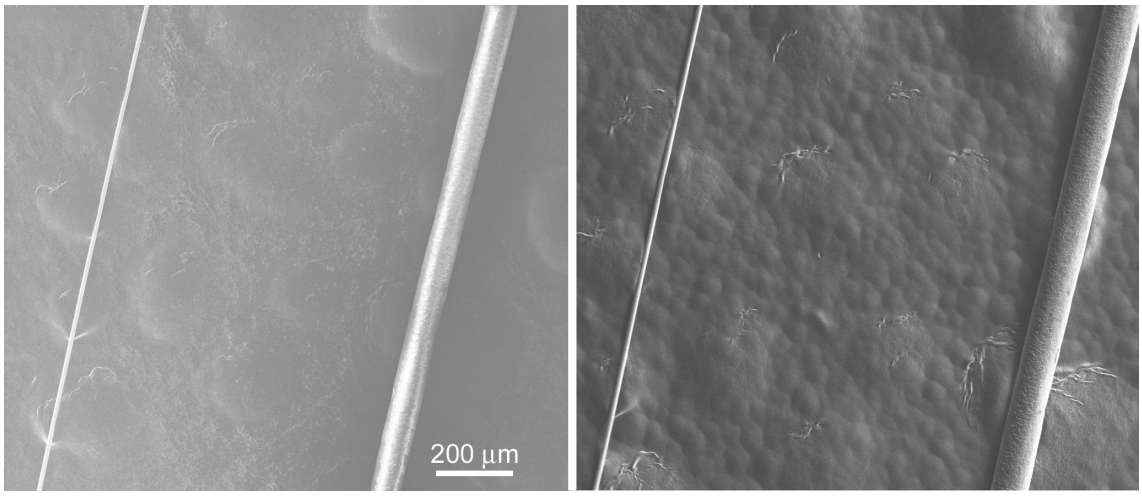

Fig. 2.8: Comparison of structure image using a) SEM system and b) FIB system. Higher contrast can be observed due to lower electrostatic surface charging at the cost of higher sample "damage". [27].

the use of ions will have a much greater effect on the sample. This influence depends precisely on their energy and on the material (atomic number of the material) of the sample. Compared to SEM, FIB imaging has the advantage of limiting the electrostatic charging of non-conductive samples (see Figure 2.8). Much more often, however, the ion beam is used to machining the material, namely to:

- sputtering/milling
- material deposition

Ions with higher energies can effectively sputter, i.e. mill or remove material from the surface of the sample on which they impact. This is a process of atomic collisions resulting in the removal of material from the volume of the sample. Due to the high level of focus, the FIB system is able to create pits, cuts, sections, or systematically remove material; all this with great precision in the order of nanometers. Milling makes it possible to create both cross-sections and structures with the required geometric properties. Because of this capability, FIB is often used in failure analysis, quality assurance and quality control, and as a precursor to transmission electron microscopy (cutting thin specimens). [28]

If a gas injection system (ussualy abbreviated as "GIS") is present in the FIB system, deposition on the sample surface is also possible. Ions can thus not only remove material, but also deposit it. Ions passing through the gas (composed of organometallic molecules) injected just above the surface of the sample disrupt its structure with their energy, break down its molecules and deposit almost pure metallic material

on the surface of the sample. However, the decomposition of the molecules is not 100%, as some organic residues are also partially applied to the surface. For that reason, it is thus possible to find even "cleaner" deposition techniques. [24]

2.3.3 Artifacts occurring during FIB operations

Since no process and operation is perfect, various imperfections can also occur during ion milling of samples. The main phenomena appearing during ion processing are the so-called "curtaining" and "rippling". [29]. These phenomena will now be described.

Curtaining Effect

Curtaining, or the waterfall effect, is one of the phenomena arising during ion milling. It manifests itself in the fact that lines or notches are visible when the structure is displayed by electron microscope. These are created in such a way that more or less material was removed at individual milling points. More generally, it is possible to say that curtaining is created by spatial variation of the sputtering rate of the sample and modulation of the current density by forward scattering of ions. This effect is most pronounced with: [29]

- porous materials
- samples with rough surface
- height steps
- composites of hard and soft materials

An example of this effect can be seen in Figure 2.9. However, the curtaining effect can be suppressed in several ways:

- hiding it (imaging using BSE signal, post processing)
- deposing a thick and uniform protection mask to smoothen surface
- using small currents
- sample stage rocking

Rippling Effect

Unfortunately, FIB milling can also produce ripple artifacts, which occur as terrace structures in the resulting cross section. The presence of such artifacts can make it more difficult to identify a defect or other features. Rippling is a function of material, ion beam, and angle; but is also controlled by chemical environment, redeposition, and aspect ratio. Ideally a material has a constant yield (atoms sputtered off per incident ion); however, no process is ideal and the etch rates do not remain constant for nanometer-scale processing. [30] The rippling is caused by:

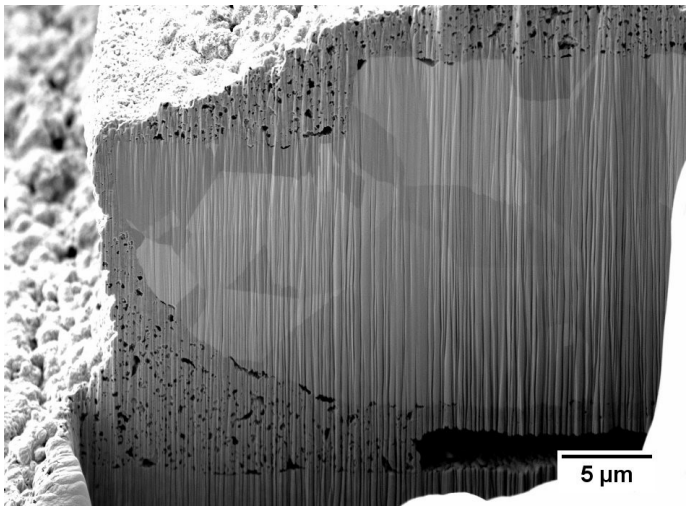

Fig. 2.9: Example of visible curtaining effect on a ion milled material. The sample is a composite of porous ceramics on nickel. The ceramics creates a very rough surface which is not uniform and the milling rate then is not uniform in the volume. [29]

- instability of process
- milled material
- ions (size of ion vs. size of atoms in solid)
- current density

It is also mostly seen in samples processed by Plasma FIB. Example of the effect is shown in Figure 2.10. But how to avoid rippling? The rocking stage will not help with this problem. To get rid of rippling it is possible to deposit a thick and very

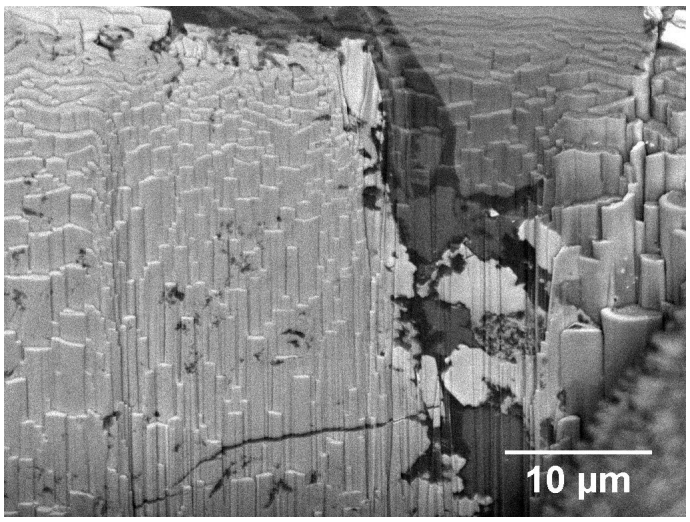

Fig. 2.10: Example of visible rippling effect on a ion milled material. The sample is a silicate rock. [29]

dense layer of platinum on the surface, or cover the region of interest with a thick piece of silicon wafer. [29]

2.4 State-of-the-art Technology and its Possibilities

Standard FIB imaging is, as mentioned several times, limited compared to an SEM system due to the destructive nature of the ion beam. SEM systems, on the other hand, offer non-destructive imaging in high resolution, but precisely because of their non-destructive nature, they are unable to machine the sample. Currently, FIB-SEM systems, so-called "Dual Beam", are widely used, where both of these technologies are integrated into a single system. By combining FIB and SEM technologies, it offers the possibility of milling the sample with an ion beam and its subsequent non-destructive imaging with an electron beam. [14]

In the field of electron microscopy (specifically FIB-SEM) there are several companies that produce these systems. Two of them, Tescan and Thermo Fisher Scientific (formerly FEI), can be included among the absolute leaders in this field. Both of these companies operate in Brno, where they were also founded. The volume of microscopes produced by these companies then exceeds 30 % of world production in the field of electron microscopy. This is why they are considered global producers. [31] However, large producers also include companies from other countries. Among them is, for example, the German company Zeiss. In the portfolio of products manufactured by this company, it is possible to find optical microscopes as well as FIB-SEM systems or X-ray microscopes. The following sections will describe the state-of-the-art technologies offered by these companies, including their parameters available in the data sheets.

2.4.1 Tescan Amber

The first in the category of SEM-FIB microscopes manufactured by TESCAN is the *Amber* device. It is a versatile microscope providing nanometer-scale imaging as well as routine FIB column operations. This makes the device suitable for precise preparation of micro-samples and characterization of various materials. The electron column provides ultra-high resolution and performance for precise analysis.

The electron source in the electron column is a Schottky FEG with a warranty of (at least) one year of operation. As for the ion column, it is possible to find a source of Ga^+ ions here. Important parameters are summarized in Table 2.1, and more details can be found in the datasheet [32]. An illustrative image of the entire system is shown in Figure 2.11.

Tab. 2.1: Some important parameters of Tescan Amber device

Parameter	Values
Electron source	0.2 pA – 400 nA
Incident electrons energy	50 eV – 30 keV
Electron beam resolution	down to 0.8 nm
Ion source	3000 μAh Ga^+
Ion beam resolution	down to 2.5 nm
Vacuum	$< 9 \times 10^{-3}$ Pa
Accessories	GIS, detectors, cameras

Fig. 2.11: Illustrative picture of Tescan Amber system [32]

2.4.2 Tescan Solaris

The second, and also more advanced, microscope from Tescan is the FIB-SEM model called Solaris. This device combines a very precise ion beam with a scanning electron microscope, which offers ultra-high resolution thanks to the immersion optics used. This precise power is then available over the entire range of electron energies.

The ion column meets the strict requirements for ion beam nanoproduction. Thanks to the automation modules, the Solaris microscope provides processing in batches or

performing some predefined operations without the need for operator supervision.

The advantage is then the large vacuum chamber, which can hold all kinds of samples of different sizes. Again, important parameters are listed in Table 2.2 or can be found in [33].

Tab. 2.2: Some important parameters of Tescan Solaris device

Parameters	Values
Electron source	0.2 pA – 400 nA
Incident electrons energy	200 eV – 30 keV
Electron beam resolution	down to 0.5 nm
Ion source	3000 μAh Ga^+
Ion beam resolution	down to 2.5 nm
Vacuum	$< 9 \times 10^{-3}$ Pa
Accessories	GIS, detectors, cameras

2.4.3 TFS Scios 2 DualBeam

The second leader in the field of electron microscopy is Thermo Fisher Scientific with its mid-range Thermo Scientific Scios 2 DualBeam system. It is an analytical system providing ultra-high resolution for a wide range of samples, including magnetic and non-conductive materials. The system provides very detailed information about the sample with sharp contrast, which can be visualized thanks to several integrated detectors, both those in the column and those located behind the objective lens.

The electron source is ensured by a highly efficient Schottky FEG gun, which provides a stable analytical current for at least two years. Of course, there are various accessories and intuitive software that even inexperienced operators can easily work with. An illustrative picture of the Scios 2 system is shown in Figure 2.12 and the important parameters are again listed in Table 2.3. [34]

2.4.4 TFS Helios 5 DualBeam

So far, the latest state-of-the-art technology from Thermo Fisher Scientific is the high-end FIB-SEM microscope of the Helios series, namely the Helios 5 FX DualBeam model. The electron beam source is equipped with technology that allows the system to reduce the energy of incident electrons below 0.2 eV, for currents up to 100 pA. This provides resolution lower than one nanometer and also high sensitivity at low energies. Imaging performance is provided by 5 integrated detectors.

Tab. 2.3: Some important parameters of Thermo Scientific Scios 2 DualBeam device

Parameter	Values
Electron source	1 pA – 400 nA
Incident electrons energy	20 eV – 30 keV
Electron beam resolution	down to 0.7 nm
Ion source lifetime	min. 1000 hod
Ion beam resolution	down to 3 nm
Vacuum	6.3×10^{-3} Pa
Accessories	GIS, detectors, cameras...

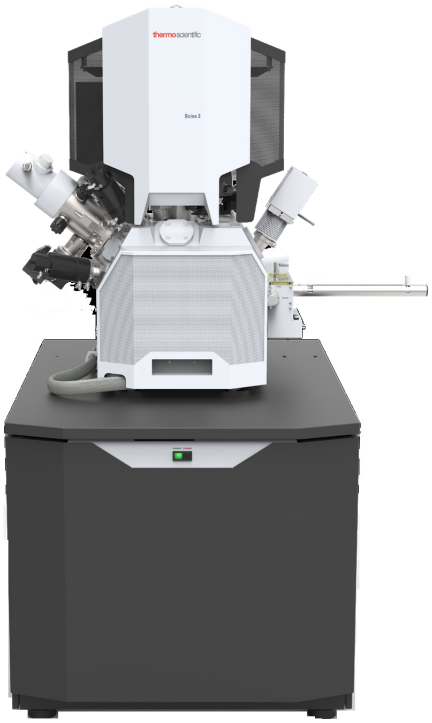

Fig. 2.12: Illustrative picture of Thermo Scientific Scios 2 DualBeam system [34]

The technology of S/TEM microscopy providing ultra-high resolution, high contrast and ultra-thin lamellae production offers complete defect and failure analysis in a single system. It is not necessary to relocate individual samples to other devices, which saves the time required for chamber ventilation and there is no need for additional separate devices for these purposes. The Helios system is shown illustratively in Figure 2.13 and its most important properties are listed in Table 2.4. [35]

Tab. 2.4: Some important parameters of Thermo Scientific Helios 5 FX DualBeam device

Parameter	Values
Electron source	1 pA – 400 nA
Incident electrons energy	20 eV – 30 keV
Electron beam resolution	down to 0.6 nm
Ion source lifetime	1000 hod Ga^+
Ion beam resolution	down to 2.5 nm
Vacuum	6.3×10^{-3} Pa
Accessories	6 chemicals, 2 GIS, detectors...

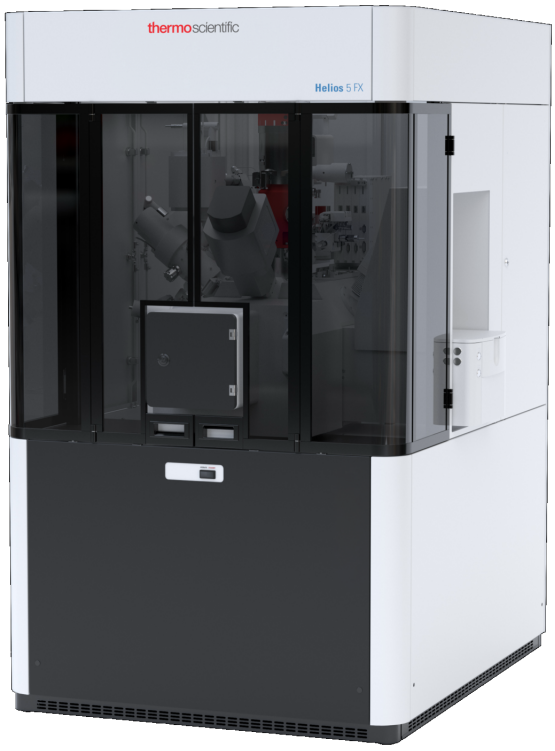

Fig. 2.13: Illustrative picture of Thermo Scientific Helios 5 FX DualBeam system [35]

2.4.5 Zeiss Crossbeam 550

The flagship of Zeiss company is the family of microscopes known as *Crossbeam*. Specifically, we are talking about the Crossbeam 550 model, which combines the powerful imaging and analysis system of a Schottky electron source scanning microscope with a new generation focused ion system. Their own optical system Gemini ensures that the examined sample is not exposed to a magnetic field, which allows

to achieve high-resolution imaging of large areas without interference and affecting the optical performance. These optics can also easily image magnetic materials.

Thanks to the expansion modules, it is also possible to connect a laser module to the microscope, thus enabling a whole range of operations for the needs of laser ablation as well as ion processing and electron microscopy in a single system, thus facilitating the need for maintenance of multiple devices. A powerful femto-second laser with airlock technology ensures cleanliness in the chamber without unnecessary contamination and quick access in the depths of electrotechnical structures in a state of high precision.

Some of the key information about Crossbeam 550 system are listed in Table 2.5. Also the illustrative picture of basic device version is shown in Figure 2.14. [36]

Tab. 2.5: Some important parameters of Zeiss Crossbeam 550 device

Parameter	Values
Electron source	10 pA – 100 nA
Electron beam resolution	down to 0.6 nm
Ion source lifetime	3000 μAh Ga^+
Ion beam resolution	down to 3 nm
Laser wavelength	515 nm – green
Laser pulses	shorter than 350 fs
Laser spot size	smaller than 15 fs
Accessories	laser module, GIS, 7 detectors, two chamber sizes

Fig. 2.14: Illustrative picture of Zeiss Crossbeam 550 system [36]

3 Laser Ablation and its Use in FA and EM

As already mentioned in chapter 1, the analysis of microscopic defects as a part of quality assurance requires access to these defects in order for them to be analyzed (usually using electron microscopy). Defects in 3D structures made of various materials, mostly installed in opaque packages, are currently being widely investigated. Access to these structures, however, requires the removal of a large amount of material. This process is generally very time-consuming, which is why there is an obvious effort to find ways to speed this process up.

One of the methods of material milling has already been described in section 2.3, but unfortunately it is not sufficiently effective for large volumes of material. In addition, FIB brings disadvantages in the form of material changes and other unwanted effects on the object of interest. Therefore, another method is often used for these purposes, namely *laser ablation*. This technology will be described in this chapter including its advantages and disadvantages and how it is used specifically in defect analysis.

3.1 Principle and Use of Laser Ablation

The principle of laser ablation consists in the impact of a powerful laser on the processed sample with very short pulses of electromagnetic radiation. These pulses last for a short time in the order of nanoseconds to femtoseconds. However, it is generally possible to use continuous lasers for laser ablation, provided that they are able to produce enough energy to overcome the ablation threshold of the material. Depending on the material being processed, laser ablation requires a specific cutting power to achieve the required depth. [37] Short pulses of the laser beam are connected to the power of the laser and the duration of them in an important characteristic of the device. This parameter will be described in subsection 3.1.2.

However, in defect and failure analysis, ablation is only used to speed up the machining process (compared to FIB). Nevertheless, due to the poorer spatial resolution, it is still necessary to use the laser in combination with the FIB, so the size of the laser machining zone must be limited in order to minimize the final time of the more time-consuming ion "polishing" process. Also, the laser is able to quickly remove a large amount of material, but it causes a lot of damage in the vicinity of the ablated area as well. The process must therefore be optimized so that this damage is as small as possible. Of course, the laser used for this purposes has different properties and parameters, which then affect the entire ablation process. These parameters, some of which can be set, include:

- laser wavelength
- laser power and pulse energy
- focal length
- beam diameter
- pulse duration
- frequency of repetitions
- number of iterations

These properties and parameters, including their effect on the ablation process, will be described individually in the following paragraphs.

3.1.1 Wavelength of the Laser Beam

One of the main properties of a laser can be considered its operating wavelength. The wavelength of the laser depends on the type of laser used. Wavelengths can range from the ultraviolet spectrum to the infrared, including the visible region of the spectrum. It is an important property, because after the impact of the beam on the surface of the processed material, part of the energy of the pulse is absorbed, while the other part is reflected. The absorbed portion of the pulse energy increases the surface temperature of the sample, thereby facilitating the ablation process; the reflected part is considered as energy loss. The *material* of the sample then determines the *ability to absorb certain wavelengths* and thus the energy of the laser. It is therefore essential to select the most suitable laser with a specific wavelength for a specific material, in order to absorb most of the laser energy and thus maximize the ablation rate. [38]

3.1.2 Power of the Laser and Pulse Energy

According to the equation for calculating the photon energy (see Equation 3.1), it is clear that the energy of the laser is dependent on its operating wavelength. Lasers with a shorter wavelength therefore produce more powerful beams. However, this is not always an advantage. The reason for this is that higher photon energy leads to more damage caused to the sample, which is linked to the creation of larger nanoparticles, which can be counterproductive to the ablation process. [37]

$$E = \frac{hc}{\lambda} \tag{3.1}$$

The energy of the pulse is also related to the mentioned pulse operating mode. Continuous mode lasers produce a continuous stream of energy without large changes in amplitude (ideally none). In this way, however, a lot of heat is also transferred to areas around the ablation target point (which is usually unwanted). In contrast,

pulsed lasers that operate in repeated "on/off" modes allow the production of laser beams with *higher energy values* while maintaining a *lower average power* value (see Figure 3.1). Thanks to this, these lasers are able to perform more precise operations and are also suitable for the ablation of heat-sensitive materials.

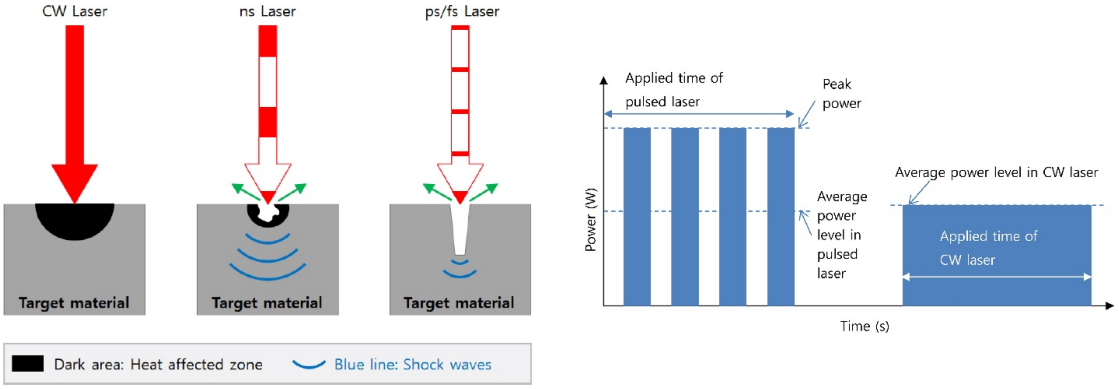

Fig. 3.1: Difference between energy values of a continuous wave laser and a pulsed lasers [39]

3.1.3 Beam Diameter and Focal Length

Beam diameter is another important parameter that determines the amount of effective energy usable in the ablation process. The smaller the spot size, the higher the energy delivered to the desired area of the processed sample. On the contrary, a larger diameter of the spot leads to the distribution of energy over a larger area, which leads to a lower energy density, i.e. to insufficient heating of the material. It is therefore important to choose a suitable lens for focusing the beam. Lenses with shorter focal lengths are better suited for cutting thin materials, while lenses with longer focal lengths are more useful for cutting thicker materials. In Figure 3.2 the difference between a correctly and incorrectly focused laser is shown, where it is important to consider the working distance of the processed sample. [38]

3.1.4 Pulse Duration

As already mentioned, pulse lengths can range from nanoseconds to femtoseconds. When the beam impacts on the sample, energy is transferred in the form of heat. The effects of a pulse of a certain duration are dependent on the cooling time of the electrons. The shorter the pulses are, the greater the difference compared to their cooling time. The larger this difference, the more negligible the electron-lattice bond, and the ablation process can then be considered a direct transition between solid and vapor. Longer pulses also cause more waste nanoparticles, which is unwanted.

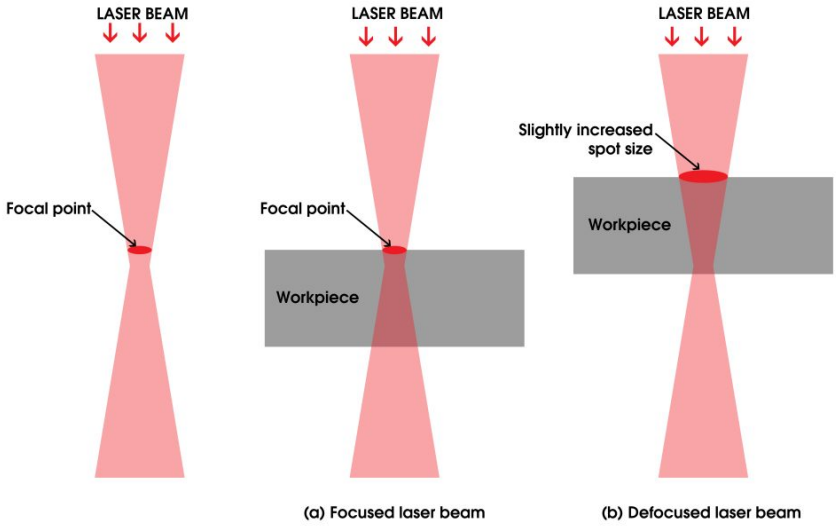

Fig. 3.2: The difference between correctly and incorrectly focused laser for the ideal ablation process [38]

.

The sizes of these particles have a greater dispersion, their shape is also less regular. However, shorter pulses result in a lower ablation yield, even though their ablation rate is higher. [37]

3.1.5 Frequency and Number of Iterations

Laser ablation frequency is the speed (number of pulses within a second) at which the pulses are sent towards the ablated sample. Also the name "pulse rate" could be used for this property. The higher this frequency, the higher the energy delivered to one point. However, for a constant average laser energy, the effective energy of a single pulse decreases with higher frequency. If the pulse rate is increased above a certain threshold, it will cause the energy of the individual pulses to not be high enough for effective ablation. This parameter must therefore be optimally set.

The last parameter associated with the laser ablation process is the number of repetitions/iterations (also the number of passes). This parameter indicates how many times the laser beam "scans" over a given area to provide the required power for machining. The higher the number of passes, the more the given area is ablated and the deeper the formed crater. [38]

3.1.6 Advantages and Disadvantages of Laser Ablation

Laser ablation uses an appropriate power setting to heat a small area of the sample that is being processed, causing material to be removed from that area. It is therefore a contactless process. One of the advantages of this process is that it eliminates the need for additional consumables (e.g. drills, ion sources...) and thus reduces the operating costs of the production process (however, the initial investment is usually higher). Laser ablation also provides an effective way to clean the surface of samples from coatings and grease. In addition, these are usually programmable devices that can be easily automated and thus increase the repeatability of production operations and decreases the need for human operators.

Among the main disadvantages of laser ablation are lower accuracy on a small scale and the temperature effect on the surroundings of the target area. The ablation process involves vaporization of the material and the formation of a large amount of nanoparticles. It is therefore necessary to use a good system to extract fumes, which could otherwise interfere with the beam and reduce the efficiency of the process. The same statement then applies to residual particles. [38]

4 Preliminary Laser Ablation Experiment

To examine the laser manipulation and the laser ablation process, a first experiment consisting of milling two microelectronic structures was performed. In the first part, several tin solder balls on the underside of the BGA package were ablated to create cross-sections, while the laser setting parameters were always differently set. In the second part, a silicon chip glued to the substrate was milled. In both cases, the goal was to find the ideal parameters of the laser settings, in order to ablate the necessary amount of material and to minimize damage to the surroundings or other layers.

microPREP PRO laser system from the company 3D-Micromac was used for both experiments. This system was made available for the purpose of the thesis by the company Tescan in Brno. The laser used operates in the visible spectrum with a wavelength of $\lambda = 532\,\mathrm{nm}$. After performing a sufficient number of repetitions, the samples were transferred to a FIB-SEM system, also on loan from Tescan, where the milled areas were enlarged using SEM (no FIB polishing was made). These areas were then compared with each other and conclusions were drawn from the observations.

4.1 Cross-sectioning of Tin Solder Balls

Within the scope of this experiment, a total of 16 trials were made, with each of them changing the parameters of the laser settings. These parameters are summarized in Table 4.1. Other parameters were then set identically for all experiments, as follows:

- ablated area: $\mathbf{0.7 \times 0.5\,mm}$
- pulse distance: $\mathbf{5\,\mu m}$
- line distance: $\mathbf{5\,\mu m}$
- number of repetitions: **125**
- scan speed: $\mathbf{250\,mm/s}$

The sample was placed in the sample holder and closed in the laser chamber. The parameters were set on the user interface display, the region of interest was located and the ablation process started. Depending on the parameters, the process took approximately from 1 min to 14 min. A different solder ball was ablated during each trial.

After the entire experiment was completed, the sample was removed from the laser device and moved into the scanning electron microscope chamber. An overview with

Tab. 4.1: Laser ablation parameters settings for solder ball experiment. The unit $p/\mu m^2$ stands for number of pulses per unit surface, FS is an abbreviation for *Focus Shift*, i.e. zooming in on the sample for focusing purposes.

#	Power	Frequency	Dosage	Pre-tilt	FS	Wobble
1	1.00 W	50 kHz	5 $p/\mu m^2$	0 °	Ne	Ne
2	0.75 W	50 kHz	5 $p/\mu m^2$	0 °	Ne	Ne
3	0.50 W	50 kHz	5 $p/\mu m^2$	0 °	Ne	Ne
4	0.25 W	50 kHz	5 $p/\mu m^2$	0 °	Ne	Ne
5	0.20 W	50 kHz	5 $p/\mu m^2$	0 °	Ne	Ne
6	0.15 W	50 kHz	5 $p/\mu m^2$	0 °	Ne	Ne
7	0.10 W	50 kHz	5 $p/\mu m^2$	0 °	Ne	Ne
8	0.50 W	70 kHz	5 $p/\mu m^2$	0 °	Ne	Ne
9	0.50 W	70 kHz	10 $p/\mu m^2$	0 °	Ne	Ne
10	0.20 W	70 kHz	20 $p/\mu m^2$	0 °	Ne	Ne
11	0.10 W	70 kHz	50 $p/\mu m^2$	5 °	Ne	Ne
12	0.05 W	70 kHz	100 $p/\mu m^2$	5 °	Ne	Ne
13	0.05 W	70 kHz	100 $p/\mu m^2$	5 °	600 μm	Ne
14	0.05 W	70 kHz	100 $p/\mu m^2$	5 °	600 μm	$30 \times 10\,\mu$m
15	0.15 W	70 kHz	100 $p/\mu m^2$	5 °	600 μm	$30 \times 10\,\mu$m
16	0.10 W	70 kHz	100 $p/\mu m^2$	5 °	600 μm	$30 \times 10\,\mu$m

all ablated regions is shown in Figure 4.1. For the purposes of creating a reference, a picture of the non-ablated ball was also taken, it is shown in Figure 4.2.

As can be seen in Table 4.1, the first 7 trials were performed with only laser power changes. It will therefore be possible to observe purely the influence of this parameter on the ablation result on these samples. The SEM image in Figure 4.3 clearly shows that with decreasing laser power and keeping other parameters constant, the amount of material removed decreases, until the point where not enough material is removed to reveal required areas.

In the next three trials, the effect of changing the dose and power on the result was examined. First, there was a simple increase in the dosage, and then a decrease in power with a further increase in the dosage. The resulting images of these three trials can be seen in Figure 4.4. It can be seen from this figure that increasing the dose alone (frame b) will allow the laser to penetrate deeper into the machined sample, but if there is a greater reduction in power (frame c), other parameters (e.g. number of repetitions) need to be adjusted.

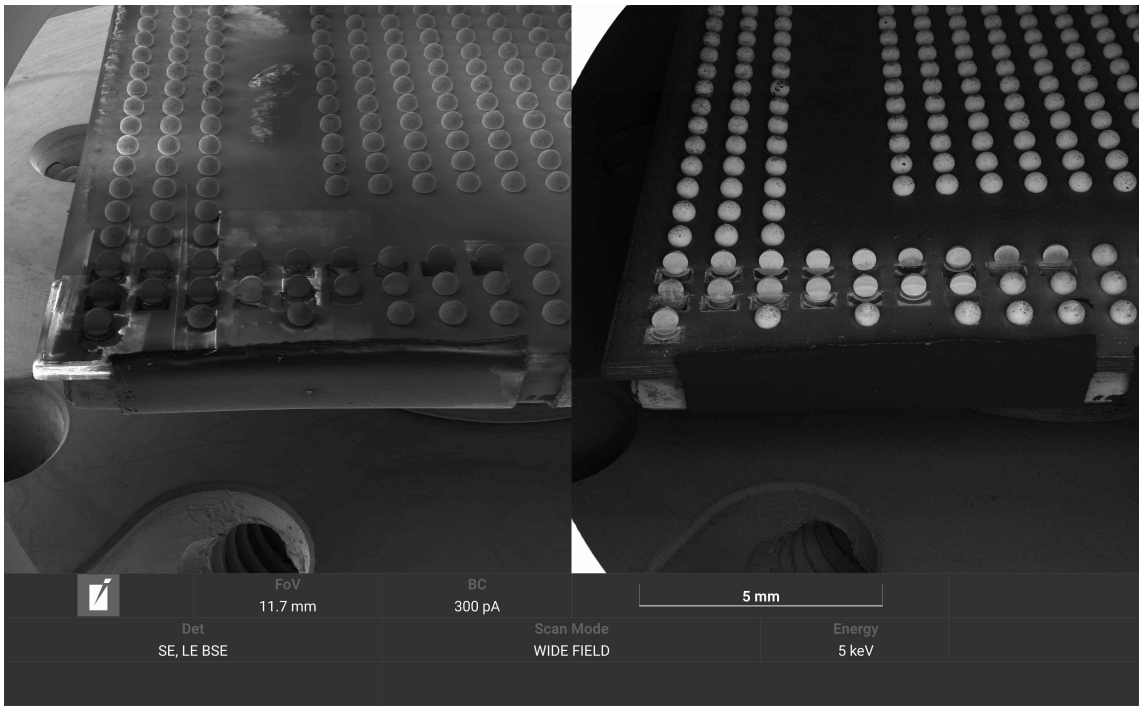

Fig. 4.1: Overview of all ablated solder ball samples. On the left, an image captured by the signal from SE, on the right, an image captured using BSE.

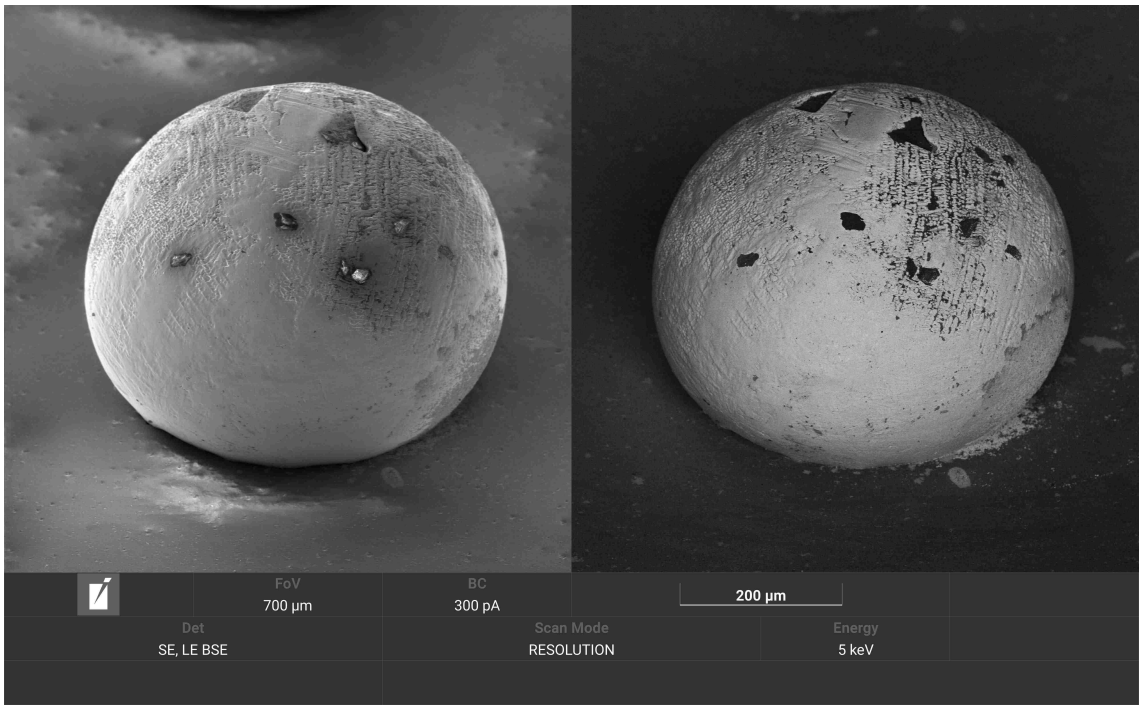

Fig. 4.2: Reference image of a non-ablated solder ball. On the left, an image captured by the signal from SE, on the right, an image captured using BSE.

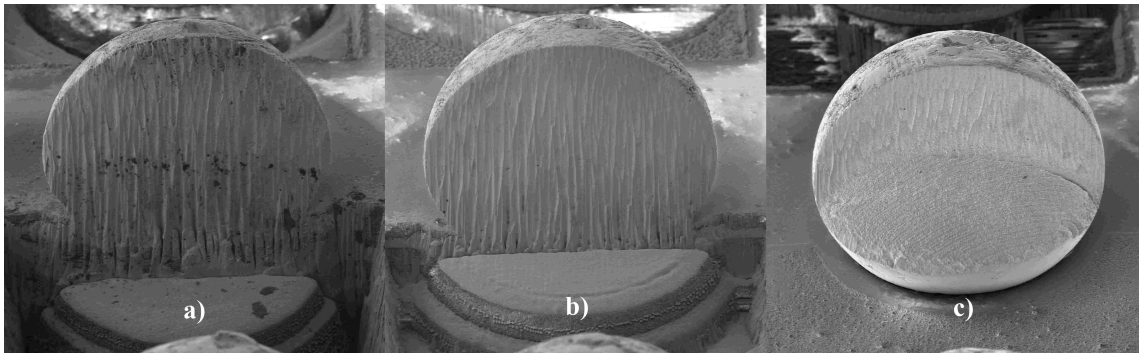

Fig. 4.3: Influence of laser power on the amount of material removed. Image captured with SE. Power needed for the results a) 1 W, b) 0.5 W, c) 0.1 W.

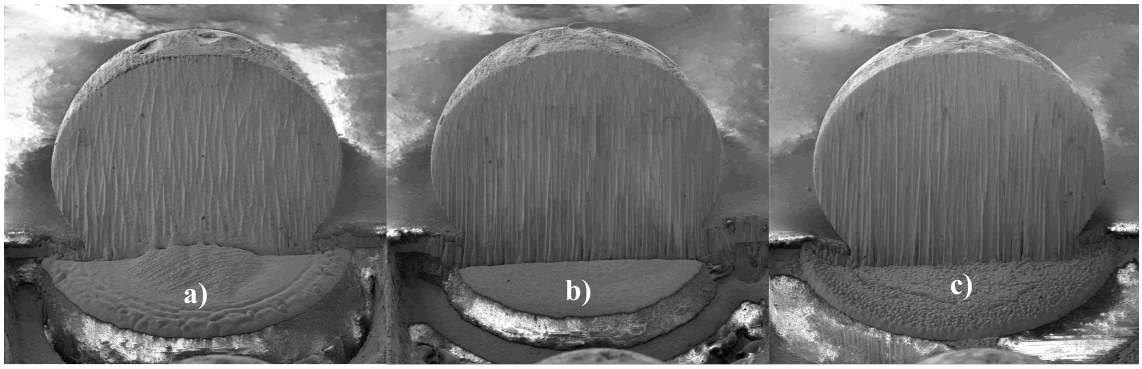

Fig. 4.4: Effect of laser pulses dosage on the amount of material removed from the surface of the sample. Image captured with SE. The dosage and power needed for the results a) 5 p/μm^2 with $P = 0.5$ W, b) 10 p/μm^2 with $P = 0.5$ W, c) 20 p/μm^2 with $P = 0.2$ W)

The remaining part of this experiment then took place with an effort to find the optimal setting of the laser parameters. The parameters were changed iteratively depending on the result of the previous trial. After viewing the image in SEM, the last attempt with setting the parameters according to Table 4.1 proved to be the most optimal. This was a setup with relatively low power but higher dose, a little tilt, beam wobbling, and a gradual decrease in working distance during the ablation process (12-level shift for a total distance of 600 μm). The resulting image of this experiment is shown in Figure 4.5.

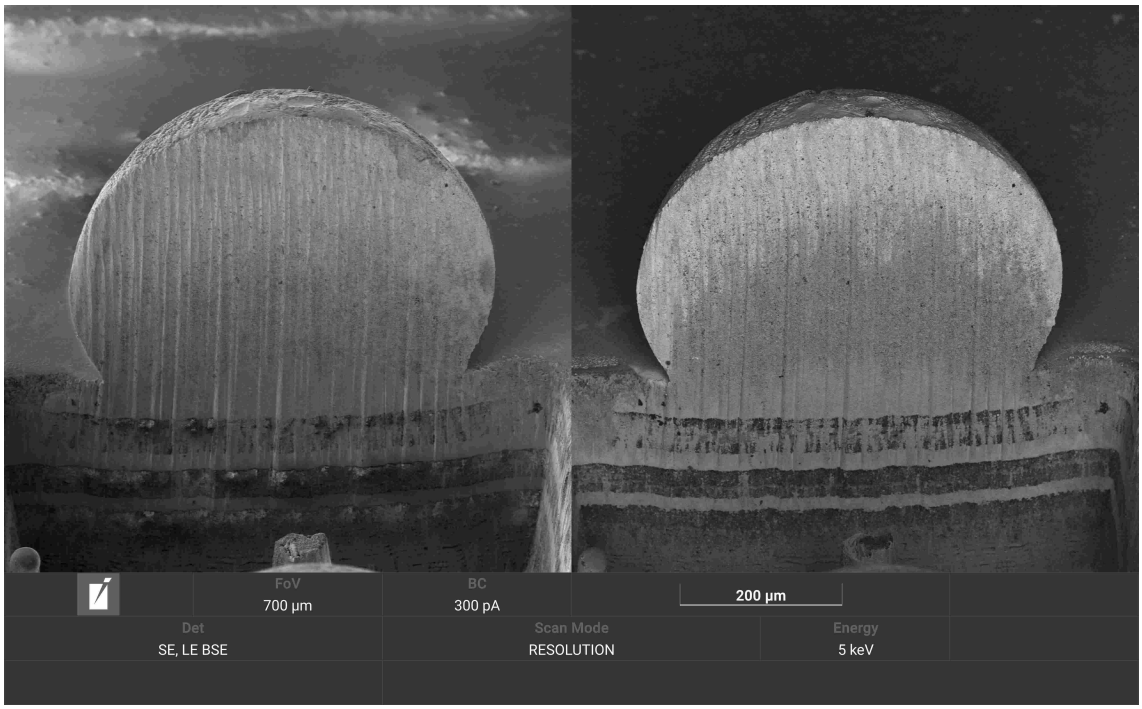

Fig. 4.5: Image showing the most optimal cross-section of the structure after an iterative search for laser ablation parameters. Left SE, right BSE.

It can be seen from the mentioned image that the sample would need to be further polished, ideally with FIB, to gain a better understanding of the structure, but the amount of material that would need to be removed is not as large compared to what was removed with a laser. A detailed image of the ball soldering area is shown in Figure 4.6, where a distinct difference in material composition and also an imperfectly flat surface can be observed.

4.2 Silicon chip milling

For the second experiment, a substrate with a silicon chip was inserted into the holder of the laser device, while the material of this very chip was to be taken.

During this experiment, 4 trials were performed. The parameters of the laser settings were again changed with each trial. The goal was to determine the effect of different settings on a different type of material. Individual trials lasted from 13 min to 19 min. An image with all created trenchces is shown in Figure 4.7.

The parameters of settings common to all trials remained almost unchanged from the previous experiment with the only exception – the size of the ablated region was set to $\mathbf{10 \times 0.7\,mm}$. The unique parameters are then summarized in Table 4.2.

Tab. 4.2: Laser ablation parameters settings for the silicon chip experiment. The unit p/μm^2 stands for number of pulses per unit surface, FS is an abbreviation for *Focus Shift*, i.e. zooming in on the sample for focusing purposes.

#	Power	Frequency	Dosage	Pre-tilt	FS	Wobble
1	0.10 W	70 kHz	100 p/μm^2	0 °	Ne	Ne
2	0.05 W	70 kHz	100 p/μm^2	0 °	Ano	Ano
3	0.20 W	70 kHz	50 p/μm^2	0 °	Ne	Ne
4	0.20 W	70 kHz	50 p/μm^2	0 °	Ano	Ano

After the end of the experiment, the sample was also moved to the SEM, where the results of all the experiments were displayed. According to the assumptions, the most material was removed during the trial with the highest power set, i.e. trials no.3 and no.4. A comparison of the amount of material removed can be seen on the image from the BSE detector for the 1st and 4th trials (see Figure 4.8). An interesting finding was then made when comparing images from the 3rd and 4th trials, the settings of which differed only in the use of focus shift and wobble. The edges of the trench, during the creation of which these parameters were used, show much greater damage and inaccuracy than the other one. This is shown in Figure 4.9

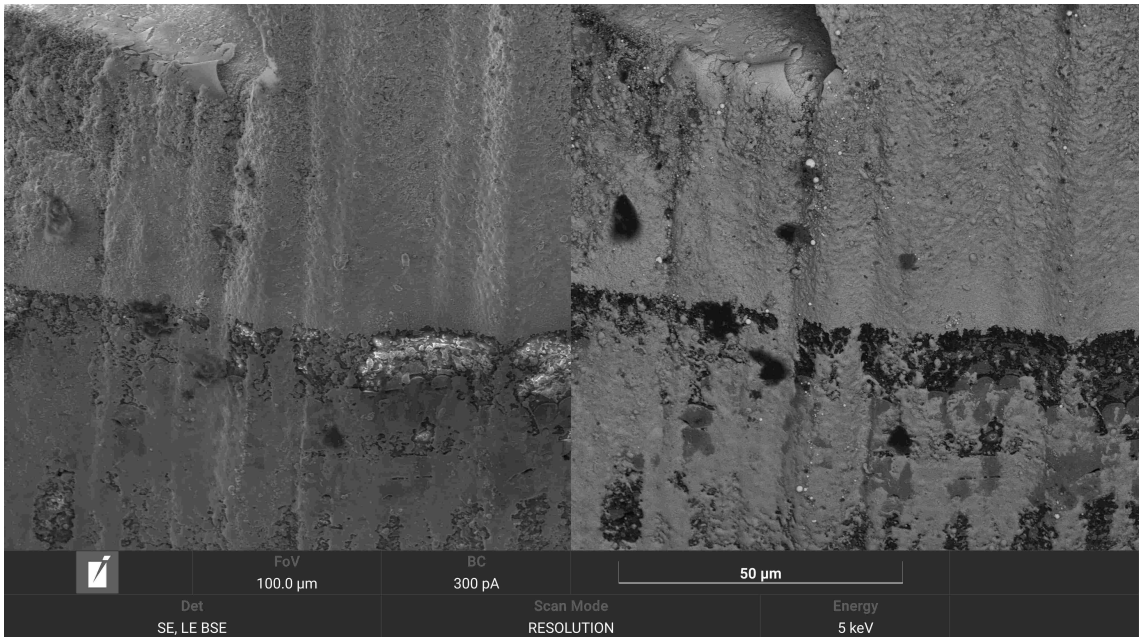

Fig. 4.6: Detailed picture of the solder ball soldering area, where the separation of the individual layers is visible. Left SE, right BSE.

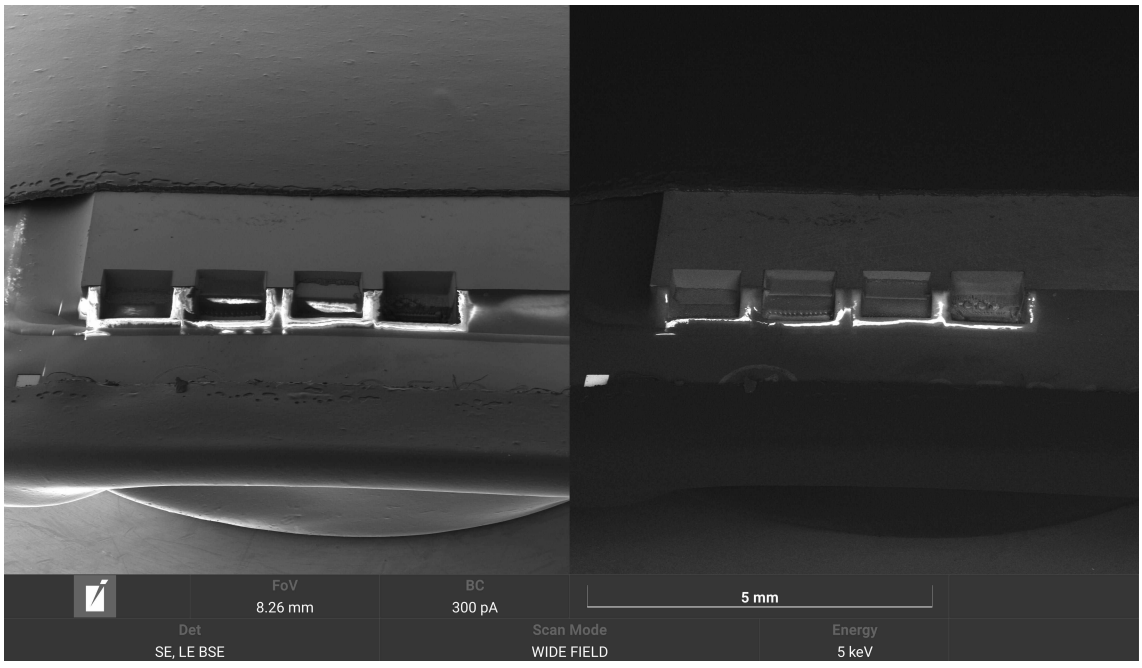

Fig. 4.7: Overview of all ablated silicon chip samples. On the left, an image captured by SE, on the right by BSE.

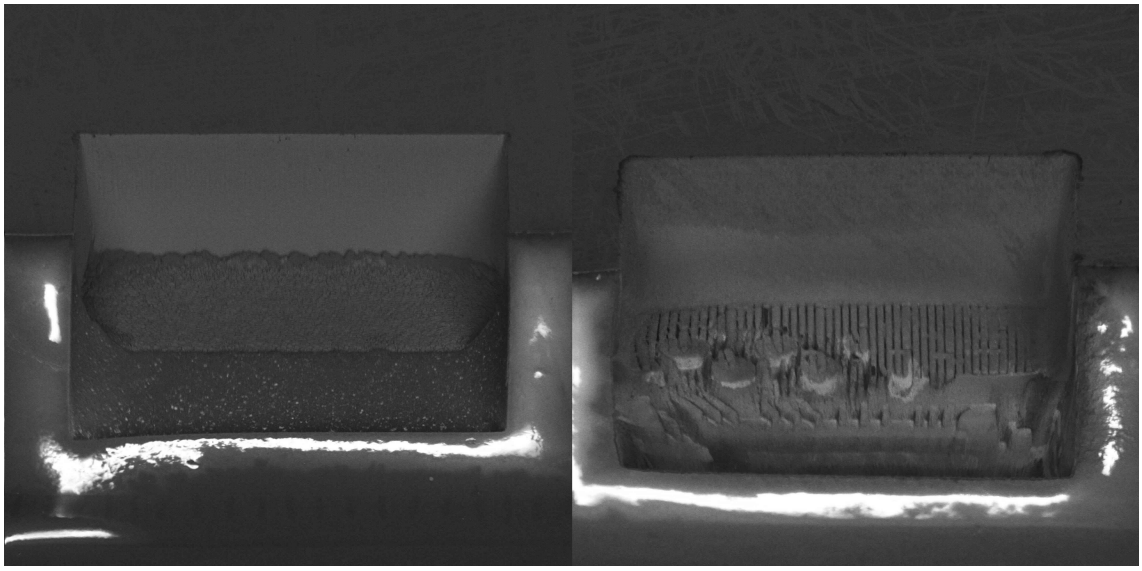

Fig. 4.8: Comparison of the amount of silicon material removed after laser ablation with a power of 0.1 W (left) and a double power of 0.2 W (right). Image taken with BSE.

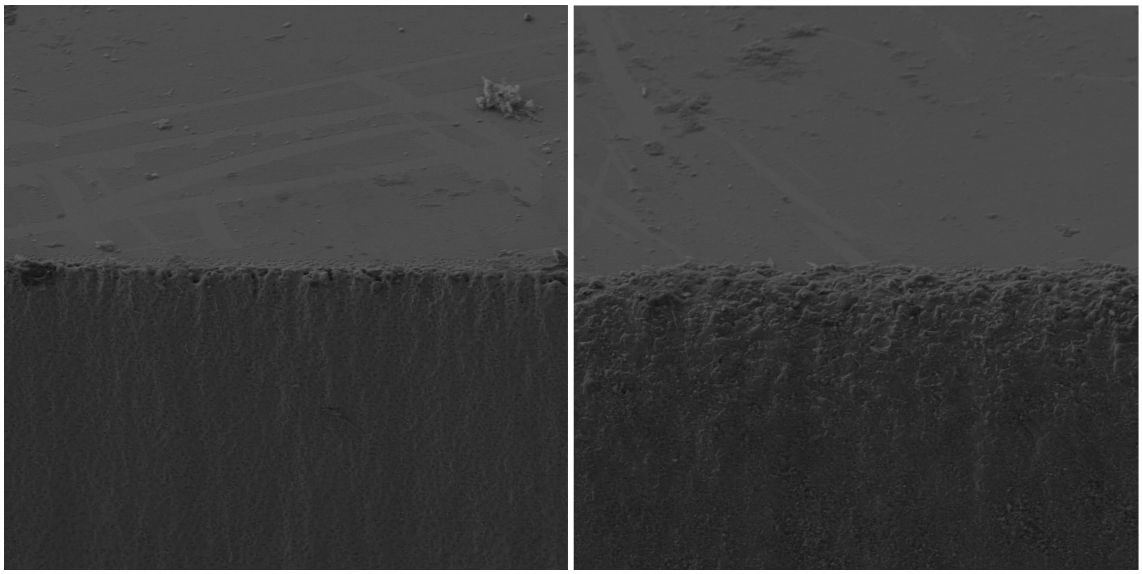

Fig. 4.9: Comparison of edge roughness after silicon ablation at the same power and with both focus shift and wobbling disabled (left) and enabled (right). Image taken with SE.

5 Defect Analysis Using Laser Ablation

After the preliminary experiment, the aim of which was mainly to test the operation of the laser, more extensive experiments were started. Several different microelectronic structures from different materials, which are commonly used in electrical engineering and are frequent subjects for QA, have been selected. With these structures, the entire process of analysis was subsequently carried out, when the sample was placed in the laser chamber, where laser ablation took place with specific parameter settings, then ion beam polishing took place in the vacuum chamber of the FIB/SEM system, and finally enlarged images were taken using an electron beam. On the enlarged images of the samples, it was subsequently observed whether the laser parameters were set ideally or incorrectly, whether the surrounding structure was damaged and to what extent, and also whether the given trenches or cross-sections reveal any hidden defects. The whole process will be described in this chapter.

Several microelectronic structures were used in these procedures:

- Solder balls
- Silicon flip chip
- Chip with wire bonds encapsulated in a package
- Ceramic capacitor

5.1 Ablation of Solder Balls

One of the samples on which the entire analysis process was carried out was again a solder ball array. These solder balls were of larger dimensions than those used in the preliminary experiment. The laser parameters for ablation of each solder ball were iteratively set according to the result of the previous trial, however, they were not recorded, and the aim of this part of the process was therefore not to determine the ideal settings for a specific type of ball joint. The aim of the laser ablation was to speed up the cross-section formation process up to the connection interface of the solder ball. From the cross-sections created in this way, the best machined ball was subsequently selected with the help of SEM, and it was then subjected to FIB polishing. Using FIB, the cross-section of this ball socket was partially polished and its defects and material composition were visualized using SEM. FIB polishing was performed to remove imperfections after laser ablation, namely curtaining.

This experiment was performed a total of seven times, an overview of all ablated solder ball can be seen in Figure 5.1. The parameters were changed so that the laser

was able to create a cross-section through the entire structure and the ball-to-pad interface could be observed later.

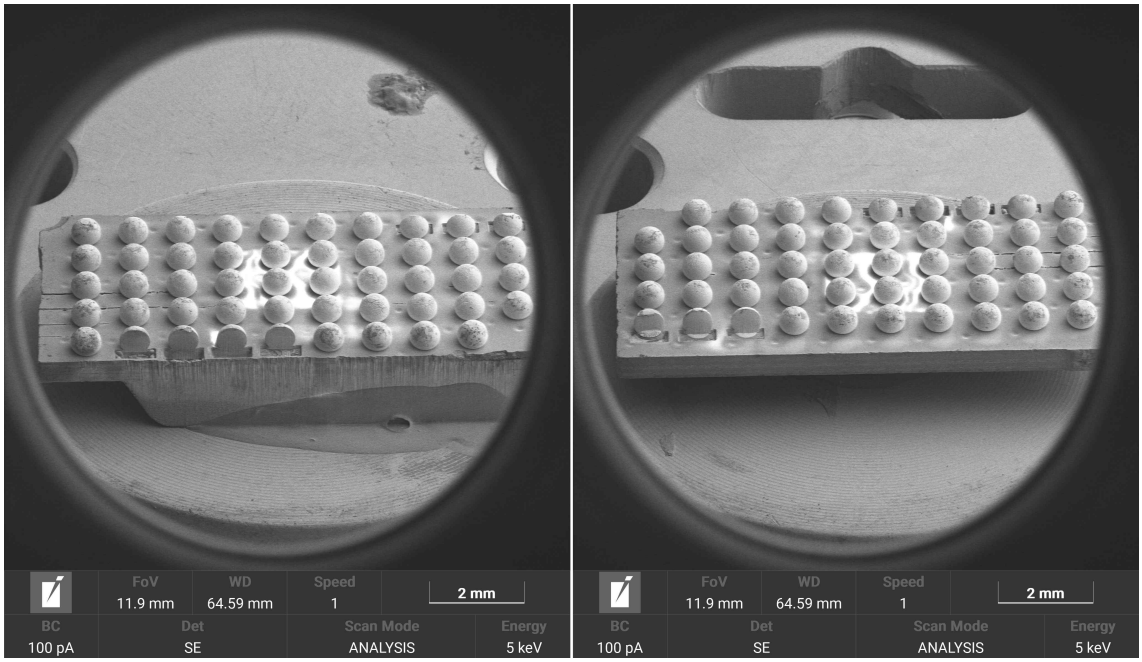

Fig. 5.1: Overview of all ablated solder balls on two sides of a substrate. Four samples in the left part, three samples in the right part.

In the SEM images, it was then possible to observe that some of the laser parameters settings were insufficient to remove enough material, so the solder pads surfaces are still hidden (see Figure 5.2a). Also with this setting, the imperfection of the laser machining can be observed, when the upper part of the solder ball shows no signs of planar processing and the deformation present could disrupt or otherwise affect the ablation process. On the other hand, the opposite phenomenon occurred for other setting, the laser parameters were too oversized and much more material was removed than was needed for the given analysis (see Figure 5.2b), while if it was a real component, it could cause unnecessary damage to surrounding structures, which is of course undesirable. Also from a time point of view, these are unnecessary delays (although in this case really negligible), which could mean big losses in other processes. However, one of the trials showed signs of approaching ideal processing. This is shown using secondary electrons at Figure 5.2c. Thus, this sample was subsequently sent to the FIB polishing process to monitor the material properties at the interface.

There is a clearly visible curtaining phenomenon on all solder balls in Figure 5.2. The cause of this phenomenon is described in subsection 2.3.3. Ion beam polishing was performed to remove it. The result of this process is depicted on Figure 5.3. The

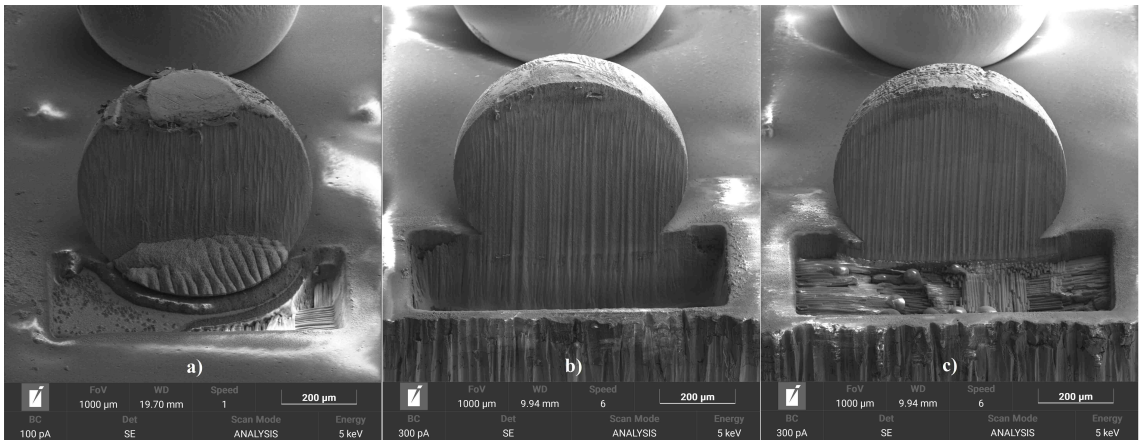

Fig. 5.2: Detailed images of some of the ablated solder balls: a) laser parameter settings were set insufficiently, b) oversized parameters and more significant curtaining, c) almost ideal result, easier to polish.

inconsistent material composition or other crystallographic impurities of the solder ball itself can be seen in this BSE image. Among other things, a layer of intermetallic compounds (usually abbreviated as "IMC") formed during the soldering of the ball is

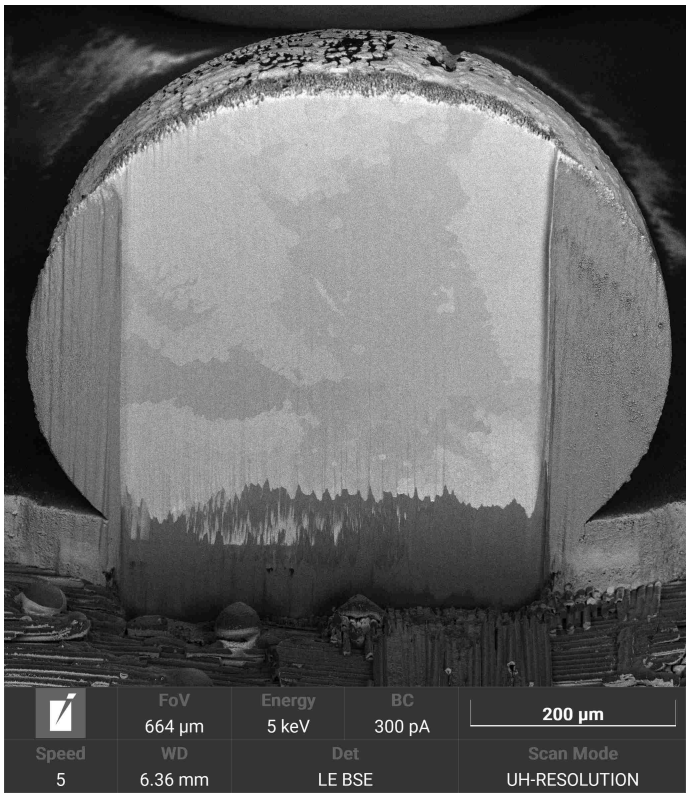

Fig. 5.3: Polished cross-section of a solder ball. Different crystalographic composition, intermetallic layers and voids/cracks are observable in the structure.

clearly visible at the interface of the solder ball and the pad. There is also an artifact in the middle part of the interface, which is probably a void (could be considered a slight defect). And at last, it is possible to observe a miniature crack in the right part of the ball foot. This defect could result in poor fixation of the component and imperfect contact.

5.2 Ablation of Flip Chip

The next processed sample was a silicon flip chip. Using the same procedure as in the previous case, 4 trenches/cross–sections were made in order to display the solder balls by which the flip chip is connected to the board and to display any possible defects in the underfill. However, 5 trenches were made, but the last laser setting was so imperfect that very little material was removed during the ablation process and the layers were not exposed to the desired depth. An overview of all 4 usable trials is shown in Figure 5.4, their further details in Figure 5.5. In the detail, it is possible to observe the exposure of the solder balls and also partially the structures to which they are attached. Several of the balls exposed this way were then selected again for subsequent polishing with an ion beam.

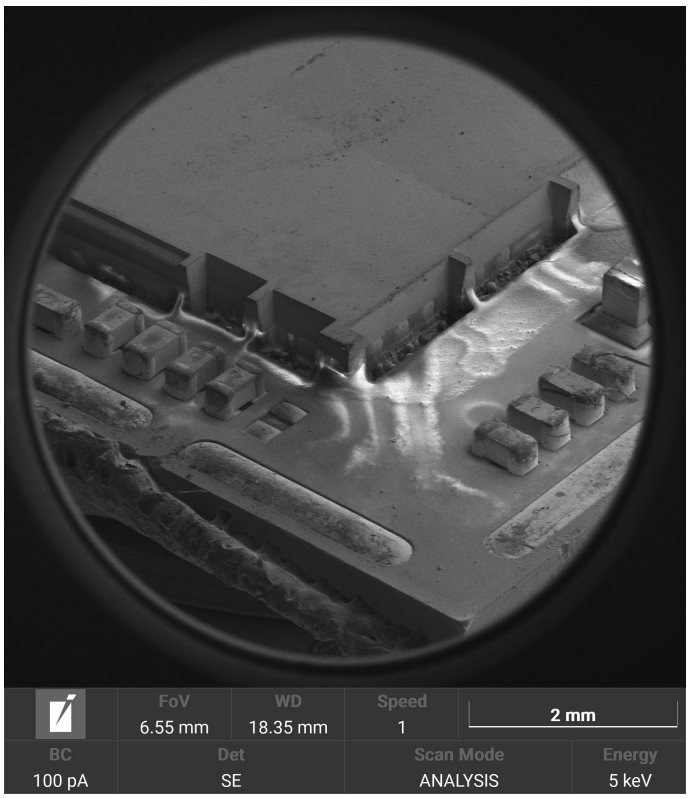

Fig. 5.4: Overview of all four cross-sections in a silicon flip chip. The purpose was to reveal the solder balls and the underfill.

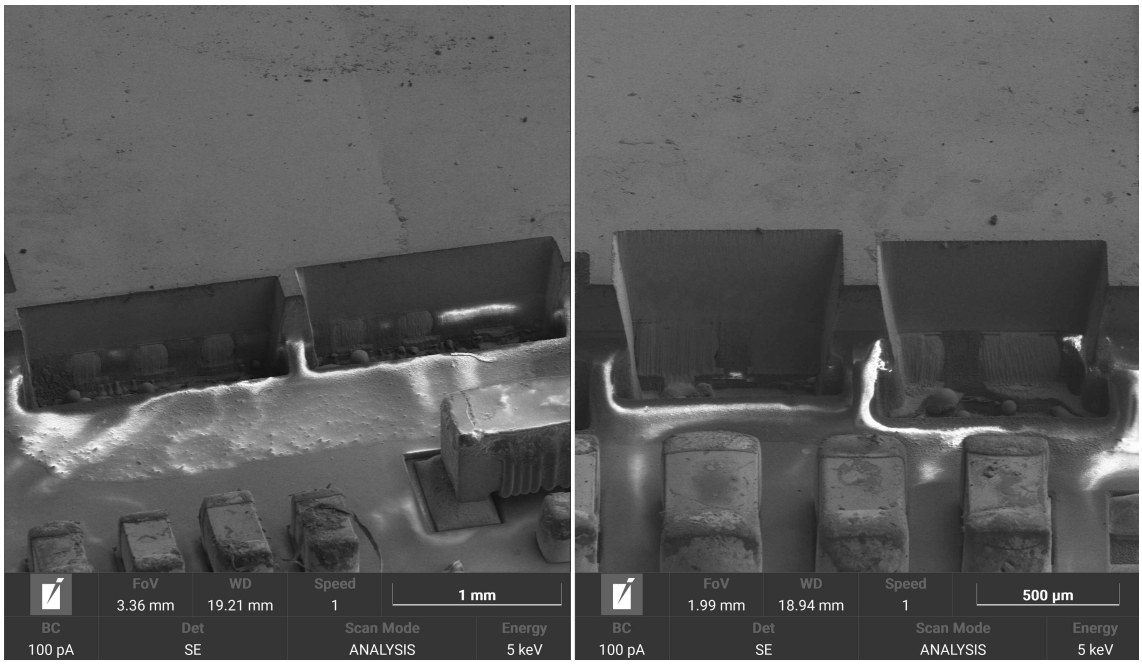

Fig. 5.5: Close up image of all cross-sections in the flip chip. Nine solder balls were revealed in total.

Due to the imperfection of the laser ablation process, two types of phenomena occurred during this experiment, namely the taper angle and the already mentioned curtaining. Both of these phenomena are visible in Figure 5.6. To eliminate these phenomena, ion beam polishing was used again. Before the actual process, however, the platinum layer was deposited using FIB and GIS. This layer was deposited in a small amount (about 10 μm) on the surface of the polished area for masking purposes. After that, the ion beam polishing process was started on a part of one of the selected solder balls. This process was carried out with Gallium ion FIB, with a restricted affection area, but even during its operation, the required areas were sufficiently polished. A comparison of the original ablated ball and the same section after this process is completed is shown in Figure 5.7.

It was possible to observe several defects on the detailed images of the exposed area using BSE, which are definitely not desirable. Figure 5.8 shows the details of the structure in the area of the terminal connection to the chip. There is visible damage to the internal structure and, among other things, also cracks and voids. Grains of other metal materials are also clearly visible on the rightmost image. These defects (metal grains are not necessarily considered defects) can contribute to the imperfect function of the entire structure and to the failure of the entire chip.

The same procedure was then carried out on the next trench. The FIB polishing process was left running until complete (this time using plasma FIB with spot size

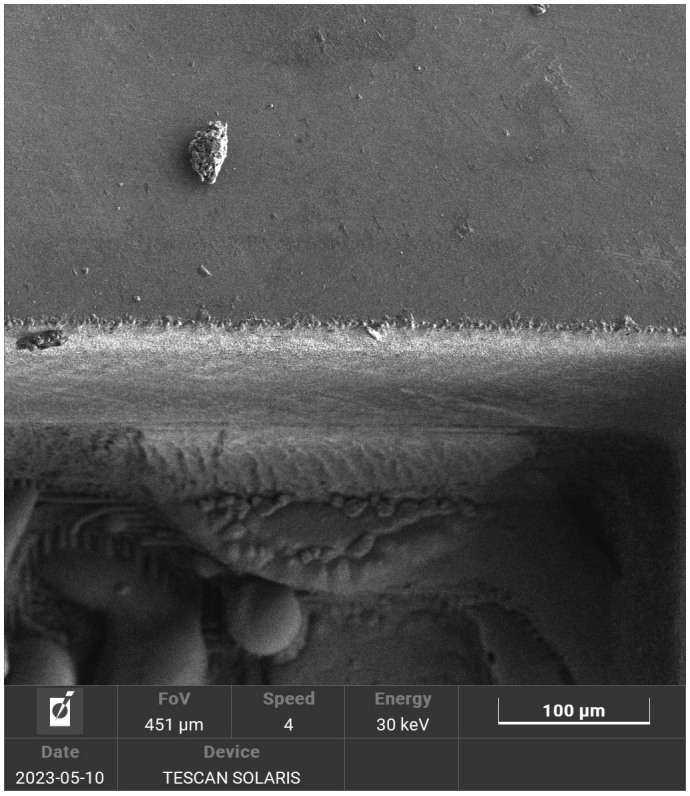

Fig. 5.6: Example of a sample with visible curtaining effect and the influence of a taper angle on an ablated sample

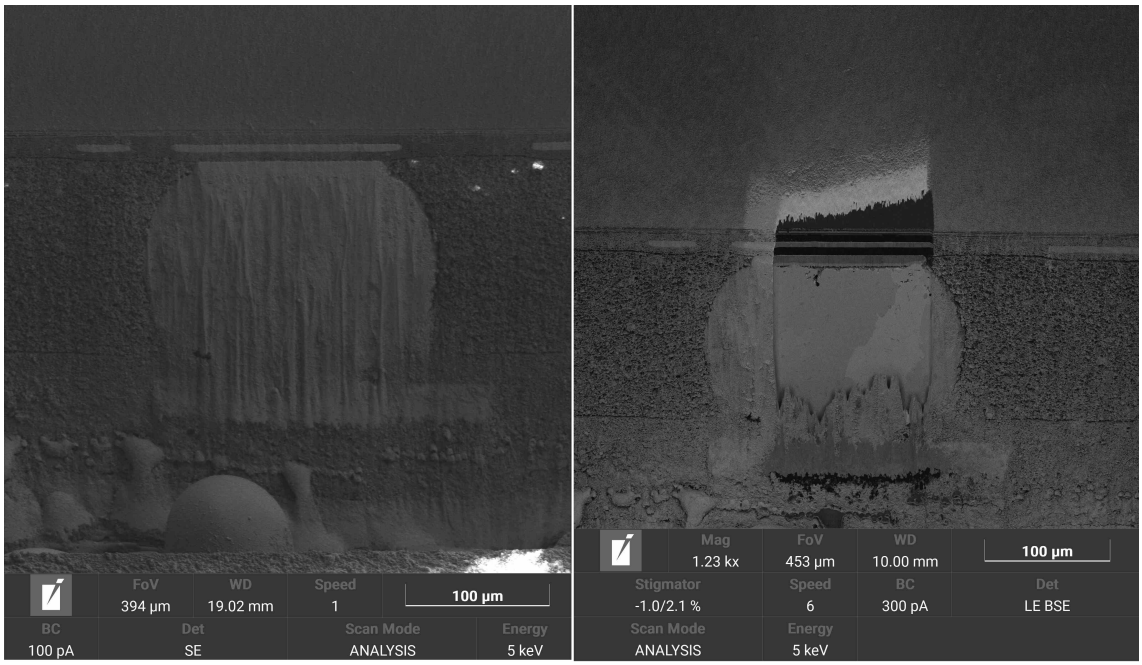

Fig. 5.7: Difference between unprocessed cross-section of a solder ball and the same ball after FIB polishing.

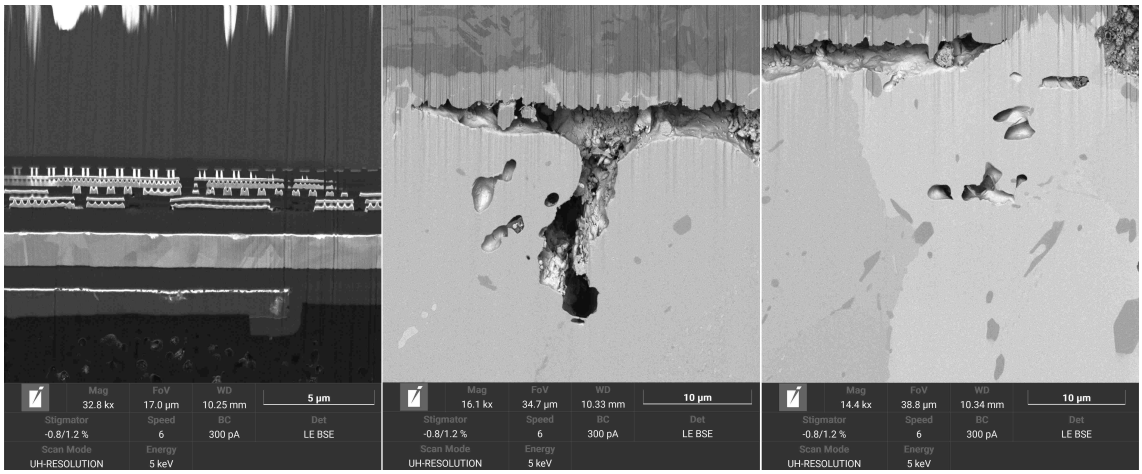

Fig. 5.8: Defects found in a solder ball structure of a flip chip. Damaged structure of a chip connection on the left; voids, cracks and metal grains in the centre and on the right.

of 1 μm) and the results are much more satisfactory than in the previous case (see Figure 5.9, the detail of both solder balls is then shown in Figure 5.10). The curtain-

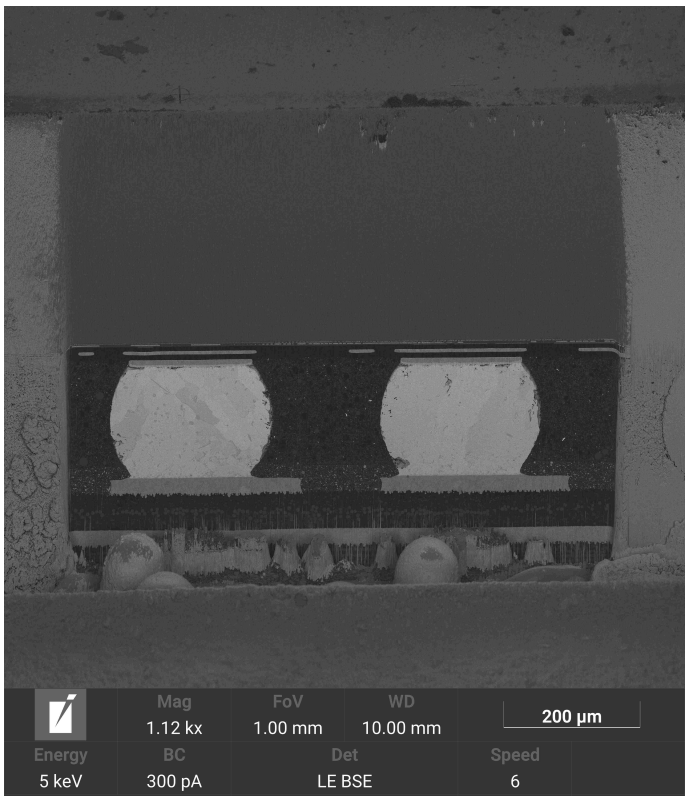

Fig. 5.9: Overview of polished cross-section of internal structure of a flip chip. Plasma FIB polishing was used with current of 1 μm.

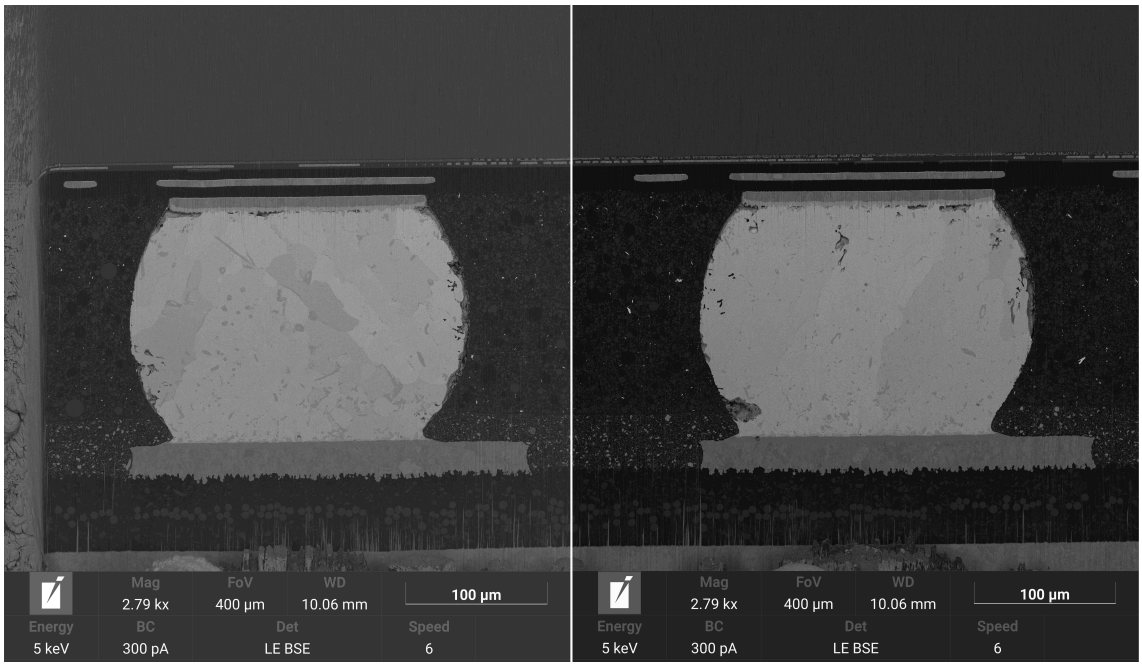

Fig. 5.10: Detailed view on both solder balls in the internal structure of the flip chip. Individual layers can be seen in both images – solder pads, chip structure, underfill, non-soldering mask, PCB etc.

ing phenomenon is much less noticeable and the whole structure shows much better contrast. Thanks to the wider selected area for ion beam polishing, it is possible to recognize defects in the underfill that remained hidden in the previous case. In the detailed images, different material compositions can be observed in the area around the lower solder pads and the rest of the underfill, as well as signs of impurities in the rest of its volume.

The more detailed images in Figure 5.11 then show imperfections and defects in the form of a gap between the solder ball and the underfill (in this case it is not necessarily considered a defect) and cracks and voids in the volume of the entire solder ball (here it definitely is a defect). The gap could have been created either during the laser machining process or, since this is a system-on-a-chip, during the manufacturing process due to heat and the associated thermal expansion effect. Overall, with this particular sample, it was noticeable how time-consuming the ion beam removal process is. Considering that the process was running for several hours (approximately 2 hours for both solder balls) and consisted only of “finishing”, it is certain that without speeding it up with the laser, the whole operation would have taken many times longer.

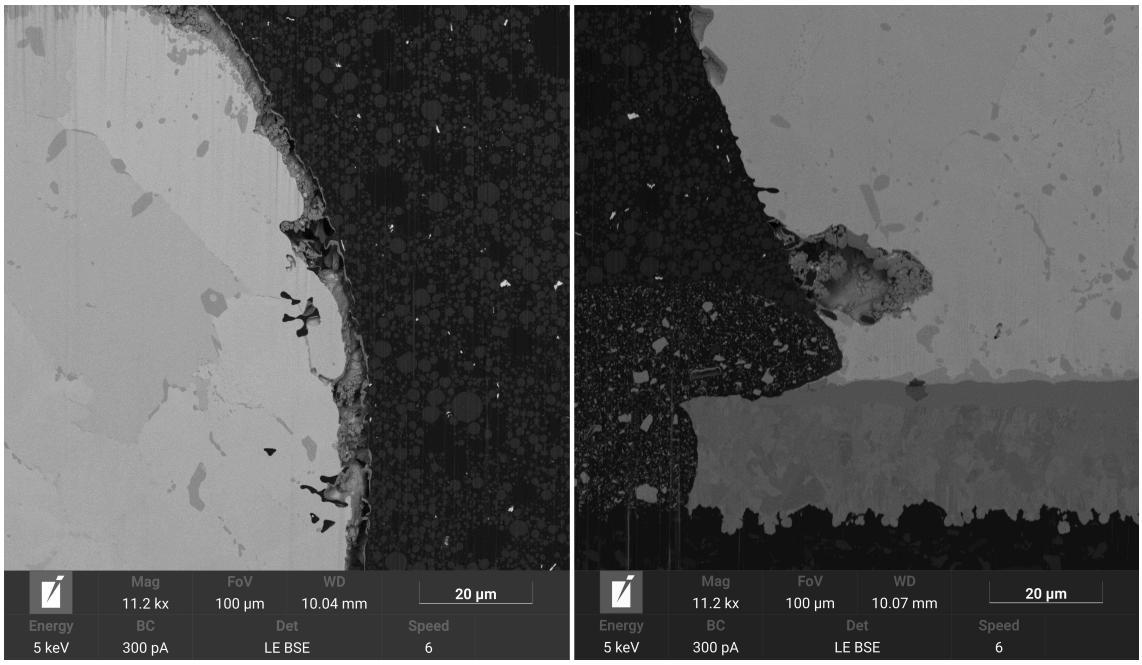

Fig. 5.11: Defects found in a solder ball structure of a flip chip. Gap between the solder ball and the underfill on the left; void and cracks on the right.

5.3 Ablation of Ceramic Capacitor

A standard ceramic capacitor was chosen as the third subject for the experiment. A total of three cross-sections were made on two different samples, however, in one cross-section the ablated region was incorrectly selected and thus no artifact is visible in the cross-section. An overview of both capacitors is shown in Figure 5.12. The picture clearly shows the effect caused by the taper angle, when the machined surface is tapered in a conical shape. Detailed images of both cross-sections were captured using SE, therefore it is not possible to sufficiently observe material anomalies in the internal structures of the capacitors, but individual internal functional capacitive layers are visible.

Figure 5.13 shows that both capacitors are of MLCC (*Multi Layer Chip/Ceramic Capacitor*) type. In the left half of the image you can see that the capacitor consist of 3 layers, while the capacitor on the other half is made up of many more ones. Since the capacitor samples did not go through FIB polishing, no defect or artifacts are apparent from the images at first glance (except for a few scratches on the soldering surfaces). For that reason, this experiment can be considered purely informative.

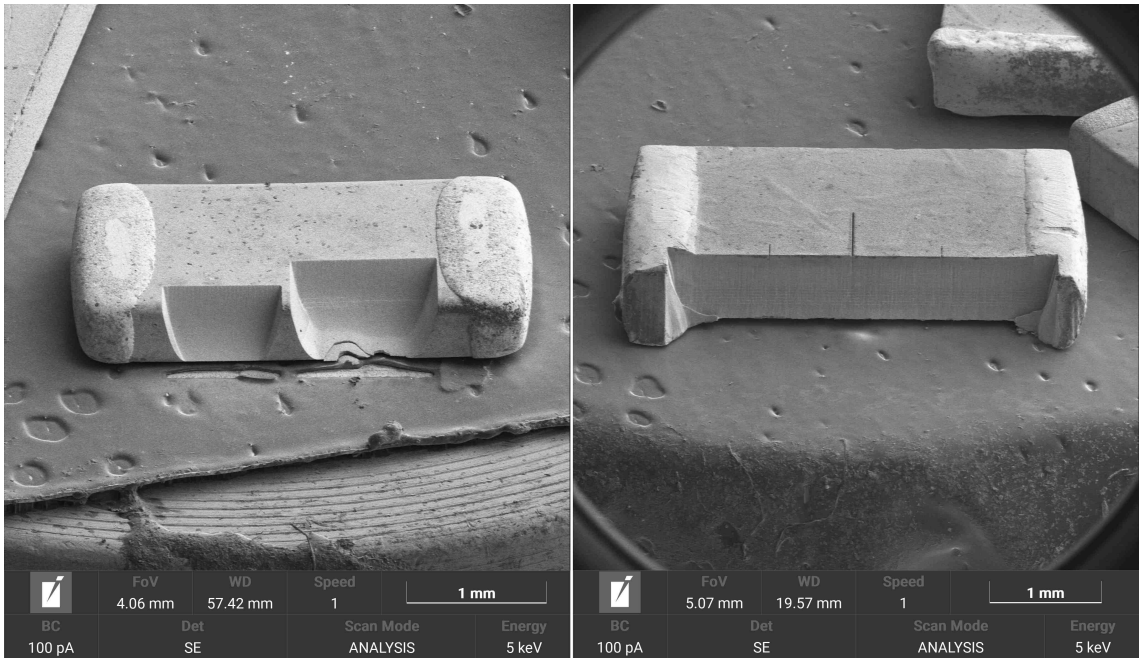

Fig. 5.12: Overview of two ablated ceramic capacitors. The influence of a taper angle is clearly visible on both samples.

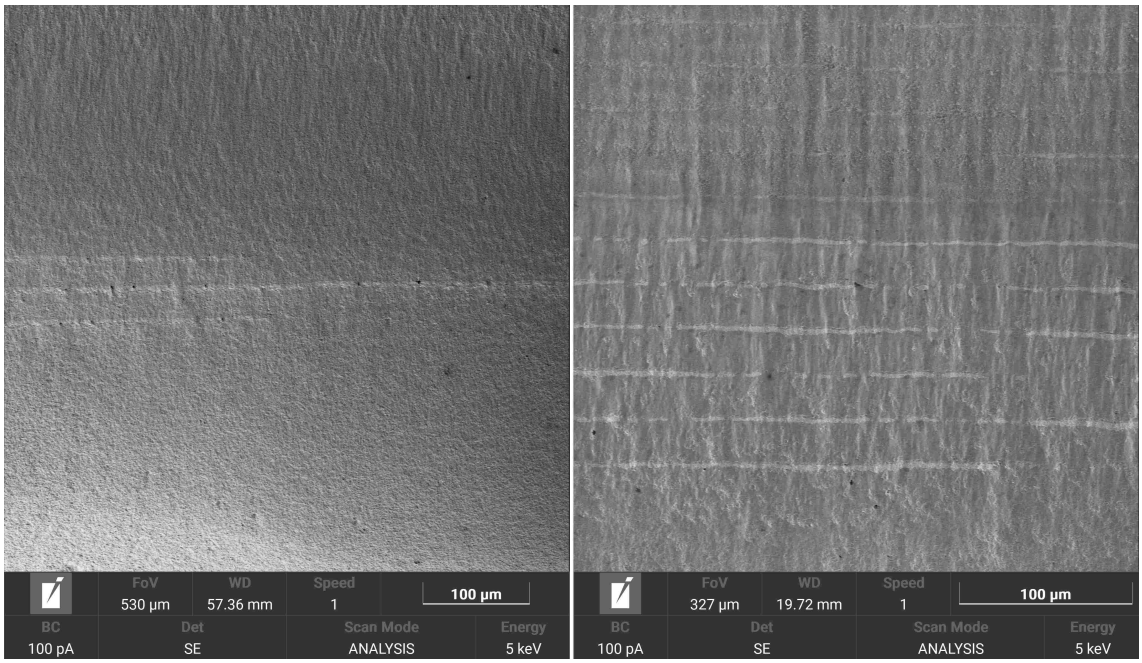

Fig. 5.13: Detail of individual layers in both multi layer ceramic capacitors. Three visible layers in the left image, many more layers in the right part.

5.4 Ablation of Encapsulated Chip

The last sample for experimental testing of laser ablation processes was a silicon chip encapsulated in a plastic package. The analysis of defects of such types of objects requires a different procedure than for the previously mentioned samples. Since the region of interest is hermetically sealed in a plastic (or other) package, it must be "revealed" to analyze such a sample. At the same time, however, it is not desirable to damage the surface or structure of the chip itself. So this experiment was about finding the ideal settings of the laser device to remove the material of the plastic case, but only to the extent that it was possible to expose the chip without damaging it. Subsequently, it was possible to analyze defects in wire bonds with which are the chip connected to the pads of the package. This process is described in this section.

5.4.1 Chip Decapsulation

First of all, it was necessary to remove the ideal amount of material to expose the wire bonds without damaging the chip itself. This experiment was repeated on two types of packages, and an overview of all trials is shown in Figure 5.14. Of these trials, only one or two can be considered successful. In the remaining trials, the parameters of the laser were either set non-ideally in such a way that the laser was not able to remove enough material to allow further analysis, or because, on the contrary, too much material was removed and the structure of the chip itself was damaged and/or even the wire bonds were destroyed.

Three attempts were made on the first type of package. Image Figure 5.15a shows the result of an ablation in which the settings of the laser parameters were overestimated and the chip was damaged. Wire bonds were also completely destroyed, leaving only the post terminals on the chip. This result is completely unacceptable for normal QA, but thanks to it, it was possible to perform further analysis described in subsection 5.4.2 experimentally. Image Figure 5.15b then shows a slightly more acceptable result. Wire bonds are still clearly visible, but the depth of penetration reaches such a level that the laser probably impacted on the structure of the chip itself and could cause damage. In contrast, image Figure 5.15c shows an ideal decapsulation where the wire bonds are exposed, but the surface of the chip is still covered by a light layer of the case material. This result is ideal for its further processing by chemical means, during which the necessary area would be sensitively revealed by selective etching. An enlarged detail of this area is shown in Figure 5.16.

For the second type of package, the ideal parameter settings for ablation were not

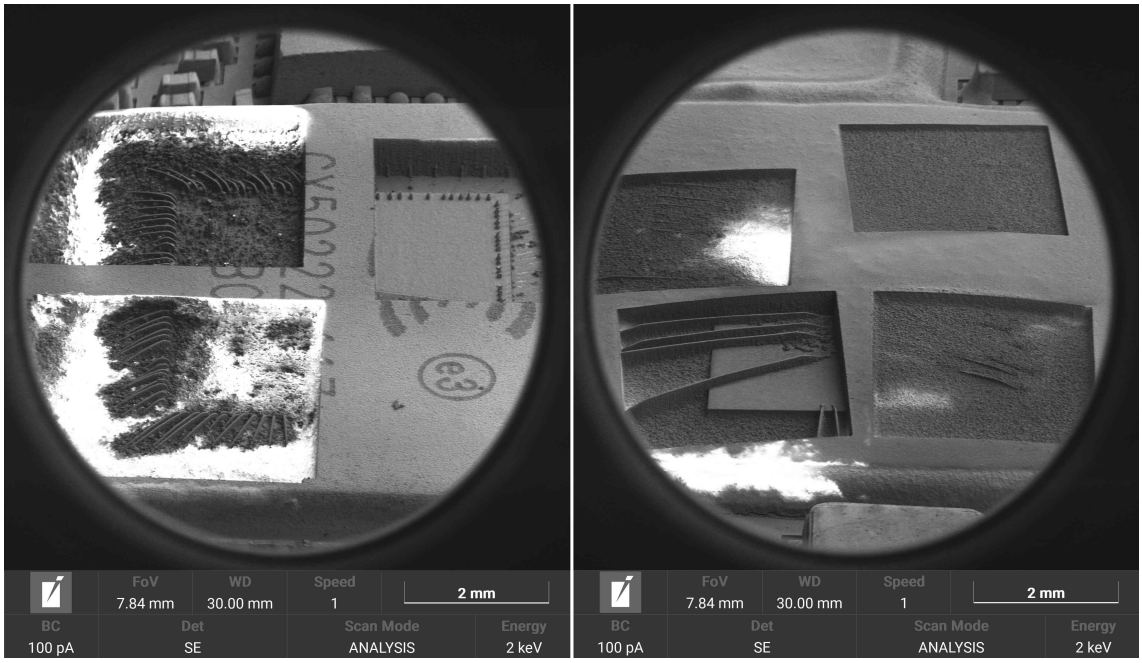

Fig. 5.14: Overview of all trials of chip decapsulation by laser ablation. Plastic package and three trials on the left, resin package and four trials on the right.

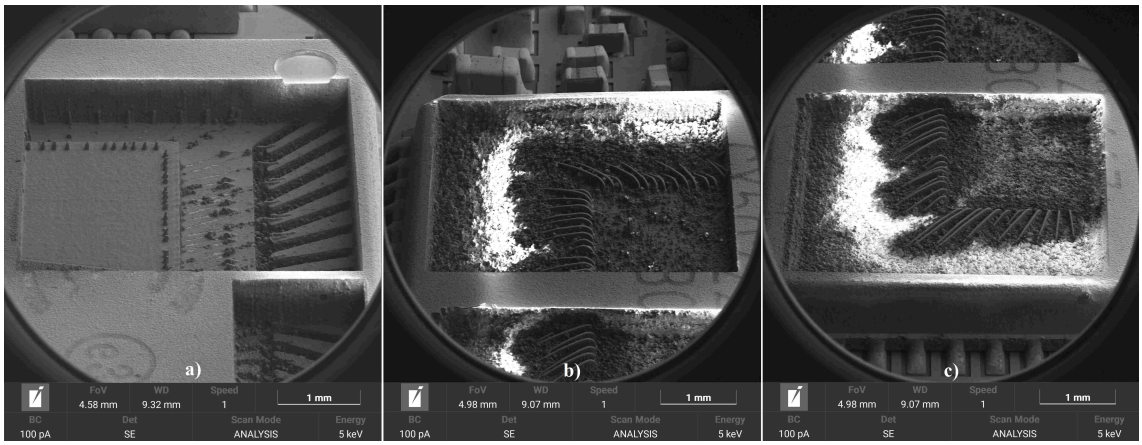

Fig. 5.15: Detail of decapsulated chips and wire bonds: a) oversized parameters, absolutely damaged chip and wire bonds; b) better laser parameters, but chip structure still damaged; c) ideal ablation result, prepared for selective chemical etching and further analysis.

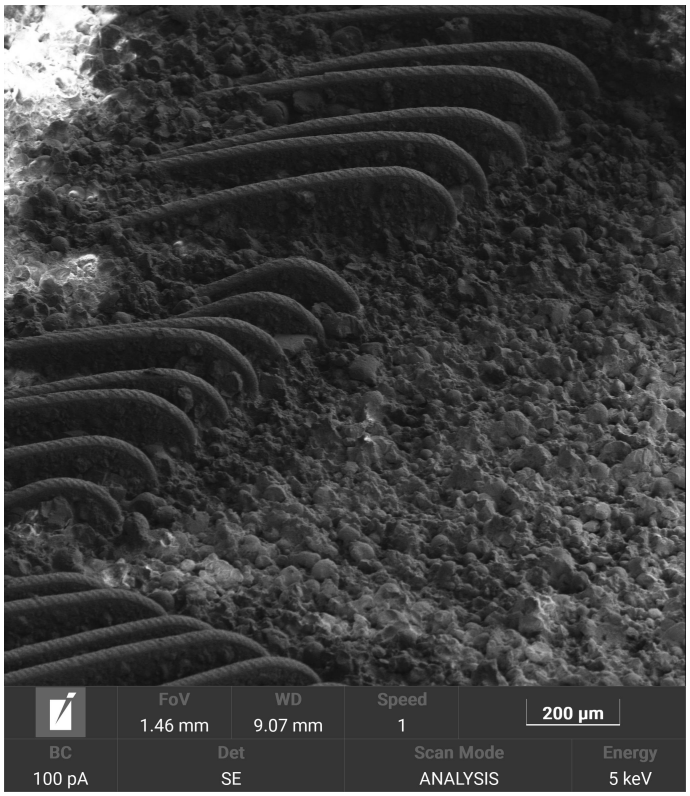

Fig. 5.16: Enlarged detail of the ideally ablated area with wire bonds.

found. The parameters of the laser were either very oversized or severely undersized. Therefore, these experiments will not be described further.

5.4.2 Wire Bond Analysis

Due to the situation where too much material was removed during the decapsulation of the package, it was possible to analyze the remaining part of the wire bond. One of the remaining objects was chosen, on which a thin layer of platinum was subsequently deposited using FIB and GIS. Then, a cross-section of this bond was created using ion milling. The result of this operation is depicted in Figure 5.17. In this image, it is visible at first glance how deep the laser penetrated the structure (a large layer of material below the pad level is gone). From this point of view, it is therefore certain that the structure of the chip was significantly and irreversibly damaged and the function layer was definitely destroyed.

In the detailed images in Figure 5.18, specific defects and impurities can be seen. A layer of intermetallic compounds formed during bonding is visible. The image on the left shows a curtaining artifact not removed during FIB polishing, as well as a heavy deposit of redeposited material under the platinum layer, which was probably created during excessive laser machining. It is probably a multi-component

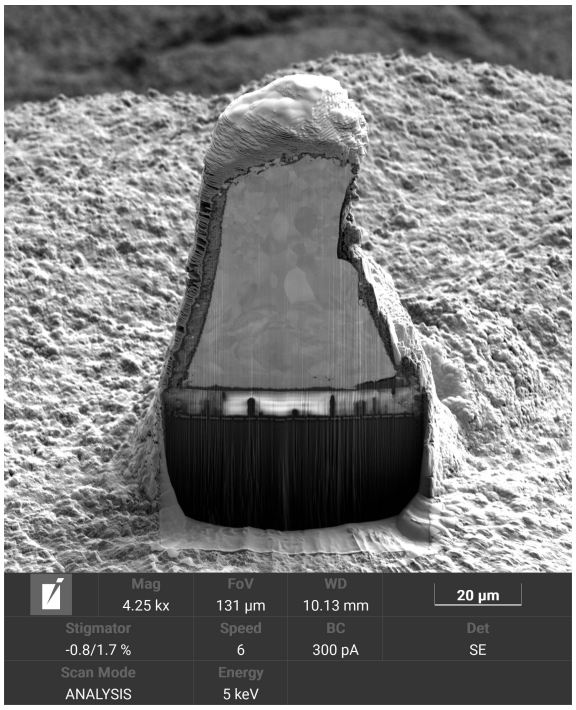

Fig. 5.17: Detail of the cross-section of the remaining part of a wire bond. The rest of the wire bond were removed by the laser ablation. Thin layer of platinum was deposited on the surface for masking purposes. It is visible that much of the chip area was removed.

resin. It is also possible to observe a crack at the interface between the joint and the pad in the lower left part of the interface. This defect was also probably caused by excessive laser machining. In the picture on the right, there is a void visible in the bond structure.

For comparison, one of the bonds revealed at the ideal laser setup was also selected for analysis (shown in Figure 5.15c). One of these bonds underwent an ion milling process, creating a cross-section of the wire. Despite the distinct curtaining effect, the structure of the joint is easily visible and can be analysed. An image of the resulting structure is shown at Figure 5.19 on the left. In the image, it is possible to observe the rather complex crystallographic structure of the wire. In the more detailed image on the right side of Figure 5.19, a gap is visible between the wire bond and the underfill, which could have been created during laser machining, as a result of thermal expansion, or during production for other unknown reasons. However, this is not necessarily a defect.

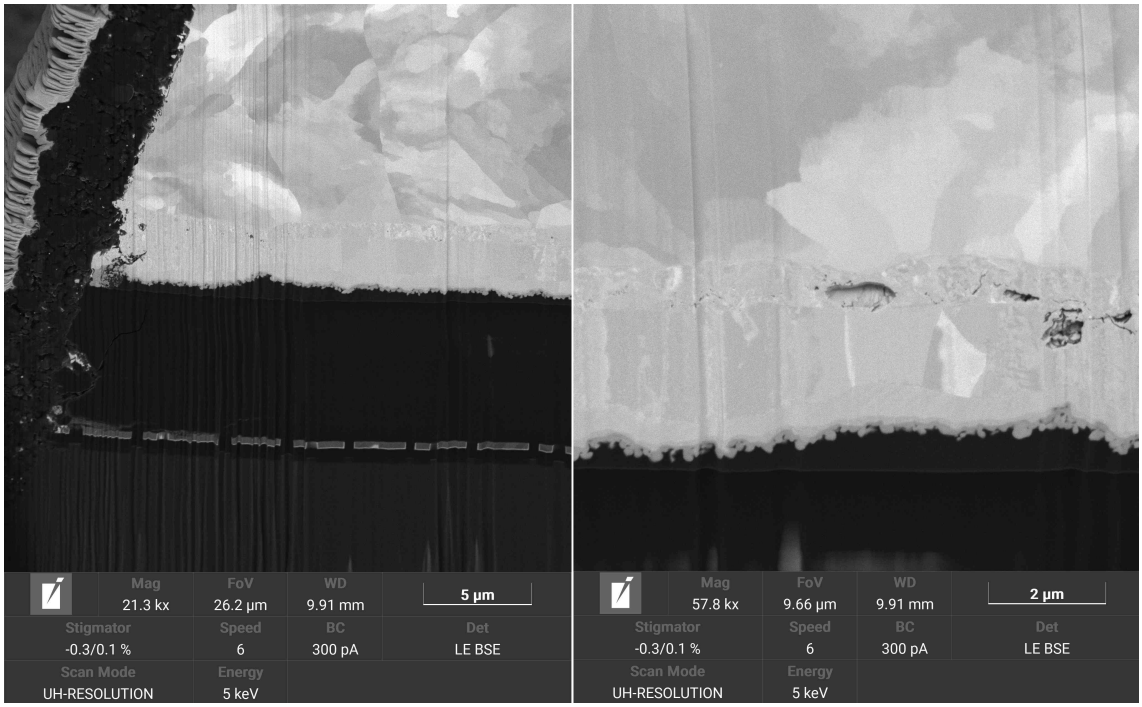

Fig. 5.18: Detail of the defects found in the cross-section of remaining part of a wire bond. Redeposition of a multi-component resin, intermetallic compounds, crack and voids.

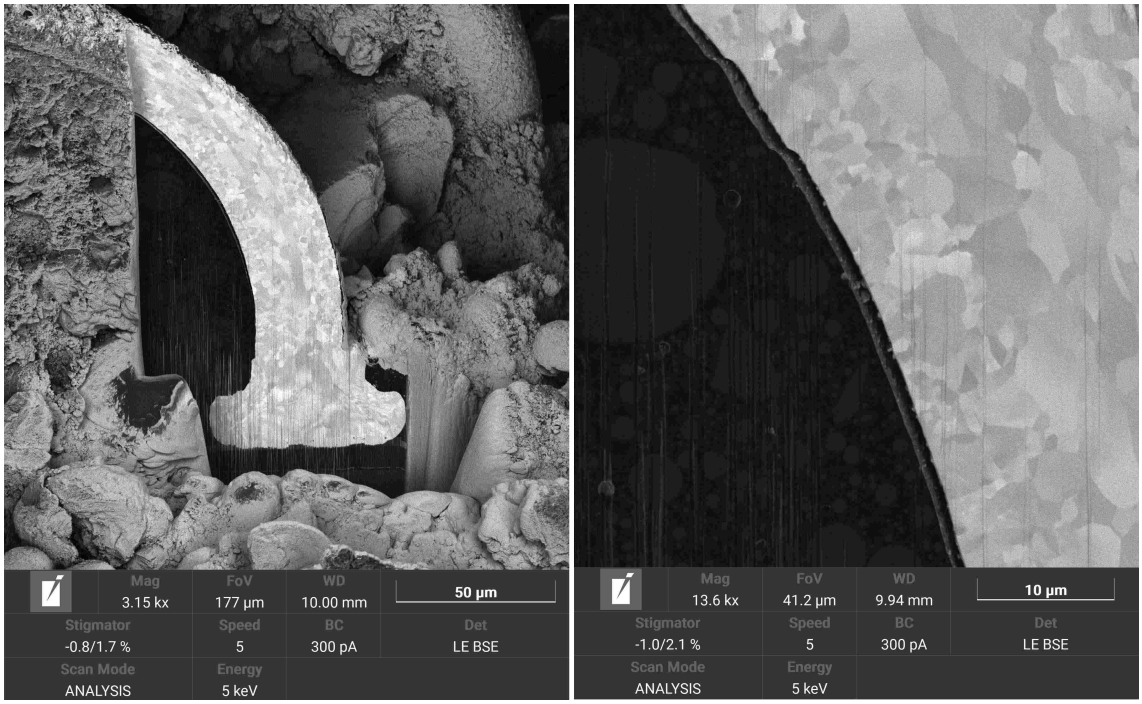

Fig. 5.19: Detail of the wire bond cross-section. BSE image shows the material and crystallographic structure.

Conclusion

This work was focused on the analysis of hidden microscopic defects in electronic and semiconductor structures. In the first part, terms such as “quality assurance”, “quality control” and “quality management” were defined, while their connection with defect analysis was explained. The second part was then devoted to electron microscopy. The general principle on which electron microscopy is based was described, and subsequently the work focused more on scanning electron microscopy, which was the subject of the assignment of this thesis. Individual components of microscopes, the way they work and what they can be used for were presented and explained. The individual processed signals and the method of their generation were also described. A special chapter was dedicated to the focused ion beam and its principle and use with regard to the topic of the thesis. Similarly, it was also the case with laser ablation and its subsequent comparison with FIB technology. The contribution of laser ablation to the work processes of quality assurance and the analysis of hidden defects was shown. At the end of the thesis, several experiments were performed, during which the influence of various parameters of the available system for laser ablation on the quality of the structure of the processed sample and its material was compared.

As part of the experiment, several trials were performed with different types of samples, and for each trial the laser system was set with different parameters. The ideal laser setting was iteratively sought to expose the desired area. Some samples were subsequently “polished” using a focused ion beam for easier analysis. The resulting machined and polished samples were then analyzed using a scanning electron microscope. Thanks to this, it was possible to observe the effect of specific parameters on the final quality of the preparation. Pictures of the individual results were also taken, and the most telling and interesting ones were subsequently presented in the thesis. By observing the course of the experiment, it was verified that different materials absorb laser energy differently and the device settings must always be adapted to the given sample and purpose.

The experiment also included the analysis of defects in exposed structures. Several impurities in terms of voids, cracks, gaps and crystallographic inaccuracies were observed. All these artefacts were shown and described in the thesis, including assumptions about their likely cause of origin. At the same time, the work verified the effectiveness of laser ablation in this industry and showed the effectiveness of such procedures.

Bibliography

[1] J. Durso. The quality assurance of semiconductor devices. *Microelectronics Reliability*, 11(2):129–137, 1972. doi:https://doi.org/10.1016/0026-2714(72)90694-4.

[2] Alexander Gillis. Quality assurance (qa). *Testing Tools & Techniques*, July 2019. URL: https://www.techtarget.com/searchsoftwarequality/definition/quality-assurance.

[3] David Carty. Quality assurance vs. quality control: Qa and qc explained. *Dev & QA Trends*, October 2021. URL: https://bit.ly/3jA2qrw.

[4] American Society for Quality. Quality assurance & quality control. online. Visited on 1.1.2023. URL: https://asq.org/quality-resources/quality-assurance-vs-control.

[5] ReQtest. Quality assurance vs quality control: Know the differences. online, June 2016. Visited on 1.1.2023. URL: https://bit.ly/3vyvgv6.

[6] Ehrenfried Zschech, E. Langer, A.M. Meyer, Hans-Juergen Engelmann, Heiko Stegmann, Holm Geisler, B. Tracyand, and Gerd Schneider. Physical failure analysis in semiconductor industry - challenges to microscopy. *Design and Nature*, 6:487–495, January 2004.

[7] Marek Tuček, Rodrigo Blando, Rostislav Váňa, Lukáš Hladík, and Jozef Vincenc Oboňa. Speeding up large-scale failure analysis of semiconductor devices by laser ablation. In *2020 IEEE International Symposium on the Physical and Failure Analysis of Integrated Circuits (IPFA)*, pages 1–3, 2020. doi:10.1109/IPFA49335.2020.9260751.

[8] Michael Davidson. Microscopyu – resolution. online. Visited on 27.12.2022. URL: https://www.microscopyu.com/microscopy-basics/resolution.

[9] Wikiskripta. Elektronový mikroskop. online, August 2020. Visited on 27.12.2022. URL: https://www.wikiskripta.eu/w/Elektronov%C3%BD_mikroskop.

[10] UMass Medical School. What is electron microscopy. online. Visited on 27.12.2022. URL: hhttps://www.umassmed.edu/cemf/whatisem/.

[11] Aryal Sagar. Electron microscope – definition, principle, types, uses, labeled diagram. online, April 2022. Visited on 27.12.2022. URL: https://bit.ly/3VBICBC.

[12] Thermo Fisher Scientific. *Exploring Uncharted Realms with Electron Microscopy*. URL: https://bit.ly/3Q8WmT1.

[13] Alex Ilitchev. How do you make an electron beam? *Electron Microscopy 101*, November 2019. Visited on 27.12.2022. URL: https://bit.ly/3WDjj3r.

[14] J. Goldstein, D.E. Newbury, D.C. Joy, P. Echlin, C.E. Lyman, E. Lifshin, L. Sawyer, and J.R. Michael. *Scanning Electron Microscopy and X-Ray Microanalysis: Third Edition*. Scanning Electron Microscopy and X-ray Microanalysis. Springer US, 2003. doi:10.1007/978-1-4615-0215-9.

[15] Matsusada Precision. Electron microscope lenses -electron microscope (sem) technical explanation series (2). *Matsusada Precision*, November 2021. Visited on 27.12.2022. URL: https://www.matsusada.com/column/sem-tech2.html.

[16] Antonis Nanakoudis. What is sem? scanning electron microscopy explained. *Electron Microscopy 101*, November 2019. Visited on 27.12.2022. URL: https://bit.ly/3Q4OphT.

[17] Charles W. Oatley. *The Scanning Electron Microscope Part 1*. Cambridge University Press, 1972.

[18] Antonis Nanakoudis. Sem: Types of electrons and the information they provide. *Electron Microscopy 101*, November 2019. Visited on 27.12.2022. URL: https://bit.ly/3Vxc1wI.

[19] Wikipedia. Scanning electron microscope. online, May 2023. Visited on 19.05.2023. URL: https://en.wikipedia.org/wiki/Scanning_electron_microscope.

[20] Wikipedia. Secondary electrons. online, June 2020. Visited on 27.12.2022. URL: https://en.wikipedia.org/wiki/Secondary_electrons.

[21] Peter Hawkes and John Spence. *Springer Handbook of Microscopy*. Springer, January 2019. doi:10.1007/978-3-030-00069-1.

[22] Thermo Fisher Scientific. *Electrons in SEM*. URL: https://bit.ly/3BLWhOX.

[23] Christian Fabjan and Herwig Schopper. *Particle Physics Reference Library Volume 2: Detectors for Particles and Radiation: Volume 2: Detectors for Particles and Radiation*. Springer, January 2020. doi:10.1007/978-3-030-35318-6.

[24] Meltem Sezen. Focused ion beams (fib) — novel methodologies and recent applications for multidisciplinary sciences. In Milos Janecek and Robert Kral,

editors, *Modern Electron Microscopy in Physical and Life Sciences*, chapter 6. IntechOpen, Rijeka, 2016. doi:10.5772/61634.

[25] Tescan Orsay. What is fib. online. Visited on 27.12.2022. URL: https://www.orsayphysics.com/what-is-fib.

[26] Wikipedia. Focused ion beam. online, December 2022. Visited on 28.12.2022. URL: https://en.wikipedia.org/wiki/Focused_ion_beam.

[27] Joseph R. Michael. Focused ion beams: How do they work and what are they good for? August 2014. URL: https://www.osti.gov/biblio/1502154.

[28] Simon Fraser University. Applications of focused ion beam. online. Visited on 28.12.2022. URL: https://bit.ly/3WJdW2z.

[29] Joakim Reuteler. Fib artifacts and how to overcome them. Online, July 2017. URL: https://bit.ly/3pXGnOO.

[30] Warren MoberlyChan. Surface modification energized by fib: The influence of etch rates & aspect ratio on ripple wavelengths. *MRS Online Proceedings Library (OPL)*, 960:0960–N10–02–LL06–02, 2006. doi:10.1557/PROC-0960-N10-02-LL06-02.

[31] Martin Rychlík. Elektronová mikroskopie, chlouba Česka. *VědaVýzkum.cz*, April 2017. Visited on 27.12.2022. URL: https://bit.ly/3WVMjmK.

[32] Tescan. *TESCAN AMBER – Product Datasheet*. TESCAN ORSAY HOLDING, 2019. URL: https://bit.ly/3vwyGi5.

[33] Tescan. *TESCAN SOLARIS – Product Datasheet*. TESCAN ORSAY HOLDING, 2019. URL: https://bit.ly/3G8Iy6r.

[34] FEI. *Scios 2 DualBeam System – Datasheet*. Thermo Fisher Scientific, 2019. URL: https://bit.ly/3Z3bGor.

[35] FEI. *Helios 5 FX DualBeam – Datasheet*. Thermo Fisher Scientific, 2019. URL: https://bit.ly/3WGS4or.

[36] Zeiss. *ZEISS Crossbeam Family – Product info*. Carl Zeiss Microscopy GmbH, 2023. URL: https://bit.ly/3MJVBjo.

[37] Maria Sportelli, Margherita Izzi, Annalisa Volpe, Maurizio Clemente, Rosaria Picca, Antonio Ancona, Pietro Lugarà, Gerardo Palazzo, and Nicola Cioffi. The pros and cons of the use of laser ablation synthesis for the production of silver nano-antimicrobials. *Antibiotics*, 7:67, July 2018. doi:10.3390/antibiotics7030067.

[38] Abraham John. Laser ablation explained: Advantages & disadvantages. *Mellowpine*, November 2022. Visited on 1.1.2023. URL: https://mellowpine.com/cnc/laser-ablation/.

[39] KangHyung Kim, Chan-Hyun Jung, Dae-Yong Jeong, and Soong-Keun Hyun. Causes and measures of fume in directed energy deposition: A review. *Taehan-Kŭmsok-Hakhoe-chi = Journal of the Korean Institute of Metals and Materials*, 58:383–396, 06 2020. doi:10.3365/KJMM.2020.58.6.383.

A The structure of the attached media

This appendix describes the structure of the DVD media attached to the thesis. The DVD contains LaTeXsource codes, an electronic version of the thesis and images from SEM in full resolution. The structure of the DVD is as follows:

```
/
├── latex ..................................... LaTeXfiles
├── images ..................................... Full resolution images
└── 195459_Valenta_Jakub.pdf ..... Electronic version of the thesis
```